# A Novel Construction Method and Control Strategy of Modular Battery Energy Storage Systems Based on Improved Droop Control

Chao Wang, *Member, IEEE*, Qiangxiang Zhang, Li Han, Yiping Xiao, *Member, IEEE*, Kang Xie, Tiezhou Wu, and Mengjun Liang, *Member, IEEE*

***Abstract*—The battery balancing technology based on modular converters needs to solve the problem of how to make many modular converters in series and parallel work together stably. In this article, according to the characteristics of modular battery energy storage systems, the application form of droop control is improved, and a battery unit with converter (BUC) is designed by combining battery, modular converter, and droop control. The properties of parallel BUCs and series BUCs are analyzed and redesigned to make them suitable for series–parallel expansion and the output current sharing control of the batteries. On this basis, a construction method of energy storage systems based on BUCs is proposed. In addition, a two-layer composite control strategy based on improved droop control is proposed, including the lower control strategy and the upper control strategy. Both simulation and physical experiments show that the proposed scheme can realize the constant voltage or constant current control of the total output of the energy storage system, and it can make the output current of each battery shared according to a given ratio with high control accuracy, and it can tolerate the communication failure of up to 2.5 s.**

***Index Terms*—Battery balancing, battery energy storage system, droop control, modular converter.**

## I. Introduction

BATTERY energy storage systems play a significant role in renewable energy generation systems, electric vehicles, and other fields. As the application of battery energy storage systems becomes more widespread, it brings more challenges and requirements for battery management systems (BMS). BMS needs to perform battery state diagnostics and provide active safety warnings [1], [2]. Battery state detection requires measurement circuits and communication circuits. If wired communication is used, it would require the addition of a large number of wiring harnesses, increasing the size and weight of the battery pack. Therefore, there is a trend toward wireless BMS [3]. Li et al. [4] summarized the current development status of the Internet of batteries. BMS also needs to have balancing capabilities. Battery balancing technology has a very important impact on the available capacity of battery pack, battery aging, and battery safety [5], but unfortunately, the existing battery balancing technology cannot meet the needs of the industry very well. At present, battery balancing technology can be divided into three categories: passive balancing technology, traditional active balancing technology, and balancing technology based on modular converters. Although the cost of passive balancing technology is low, the efficiency is also very low [6], [7]. Nowadays, most of the papers on battery balancing belong to the traditional active balancing technology [8], [9], [10], [11], [12], whose essential feature is to transfer energy from some batteries to other batteries of the battery pack, so that the energy of the batteries can be balanced. The traditional active balancing technology has the following problems that are difficult to overcome: it needs to add complex and additional balancing circuits, which increases the cost of energy storage system. There is a certain loss of energy in the process of transfer, which makes the efficiency of energy storage system decline. The works presented in [13], [14], [15], [16], [17], [18], [19], [20], [21], [22], [23], [24], and [25] belong to balancing technology based on modular converters. The characteristics of balancing technology based on modular converters are as follows: many low power modular converters are used to replace the high-power centralized converter, and each modular converter is connected to a battery. The modular converter can be used for two purposes: it cannot only regulate the output power of the connected battery to achieve battery balancing but also regulate the total output voltage or current of the energy storage system [13], [14]. Therefore, the balancing technology based on modular converters is expected to eliminate the "additional" balancing circuits and effectively reduces the cost of energy storage systems; moreover, the energy of the battery is directly transferred to the load; in most cases, there is no need to transfer energy between batteries, so the balancing technology based on modular converters has no

Received 7 October 2024; revised 31 January 2025; accepted 6 March 2025. Date of publication 14 March 2025; date of current version 26 May 2025. This work was supported in part by the National Natural Science Foundation of China under Grant 51677058, in part by the Natural Science Foundation of Hubei under Grant 2023AFB992, and in part by the Hubei Provincial Department of Education Youth Talent Project under Grant Q20231410. Recommended for publication by Associate Editor D. Oliveira. *(Corresponding author: Chao Wang.)*

The authors are with the Hubei Key Laboratory for High-efficiency Utilization of Solar Energy and Operation Control of Energy Storage Systems, Hubei University of Technology, Wuhan 430068, China (e-mail: wangc@hbut.edu.cn; 102210390@hbut.edu.cn; 102100234@hbut.edu.cn; yp_x@hbut.edu.cn; 2110631107@hbut.edu.cn; wutiezhou@hbut.edu.cn; liangmengjun@hbut.edu.cn).

Color versions of one or more figures in this article are available at https://doi.org/10.1109/TPEL.2025.3551615.

Digital Object Identifier 10.1109/TPEL.2025.3551615

additional loss of energy transfer [15]. Therefore, the balancing technology based on modular converters is expected to overcome the problems of high cost and reduced efficiency of the traditional active balancing technology in principle. However, the balancing technology based on modular converters needs to solve the control problem of many series–parallel modular converters.

For the control problems of many series–parallel modular converters, from the perspective of the overall control methods used, the existing research can be divided into three categories: centralized control, distributed control without communication, and distributed control with communication. Centralized control [13], [16] uses a central controller to control all modular converters, which has the advantages of simple control algorithm and high precision but has the disadvantages of complex connection, inconvenient for large-scale expansion, and the whole system cannot work when the central controller fails. The distributed control without communication [17], [18], [19] adopts the droop control method and adjusts the droop resistance coefficient according to the specific function of SOC to achieve SOC balancing. Literature [19] also realizes constant voltage control of output voltage, but strictly speaking, literature [19] uses a global voltage detection circuit, which is equivalent to adding a communication circuit. The advantage of distributed control without communication is that it will not be interfered by communication failure and has high stability but its disadvantage is that the control accuracy is low. In addition, because the battery energy storage system needs to monitor the status of each battery, there is a need for communication. Therefore, distributed control without communication is not compatible with the needs of battery energy storage systems.

Compared with the previous two control methods, the distributed control with communication [15], [20], [21], [22], [23], [24], [25] is the technical route with the most literature and the most development potential. The schemes without droop control [15], [20] let each converter to work in the voltage source or current source mode, and then set and schedule the voltage sources and current sources. This type of schemes has high control accuracy but has high requirements for communication reliability. When the communication delay or fault occurs, the system cannot work normally, and there are potential safety risks in the battery energy storage system. The adaptive droop control based on communication is adopted to improve the control accuracy and stability [21], [22], [23]. The influence of communication delay on control performance is analyzed in the experiment [22]. When the communication delay is no more than 20 ms, the system performance is acceptable, but when the communication delay is 1 s, the system oscillates and cannot work normally [22]. The aforementioned literature only analyzes the simple modular converter system in series or parallel. The modular converter system in series–parallel is discussed in [24] and [25], the hierarchical control architecture is proposed, and inside the battery module, the centralized control method for the battery power unit in parallel is used, and between modules, the leader/follower control and droop control based on communication is used. Both the proposed schemes need highly reliable communication support.

For the control problem of many series–parallel modular converters, the existing research still has the following two points to be improved.

1) Droop control has been applied in some fields, such as control of ac/dc microgrids and control of grid-forming inverters. These application fields are single-layer parallel or series systems. Unlike these application fields, modular battery energy storage systems are usually multilayer series–parallel systems, and their connection relationships are much more complex than those of single-layer parallel or series systems. In the field of modular battery energy storage systems, most of the literature mentioned above also adopts droop control schemes but these schemes do not find the optimal variant of droop control according to the characteristics of modular battery energy storage systems. It is necessary to find a more suitable variant of droop control for modular battery energy storage systems.
2) The distributed control based on droop control with communication is the most potential technology route but the adaptability of the existing schemes based on this technology route to communication failures is not good enough. As pointed out in [22], the proposed scheme can work normally only when the communication delay is not greater than 20 ms. The battery energy storage system has a large number of nodes and has high requirements for stability and safety. Communication delays and failures are common phenomenon in the communication field. If the system fails to work normally in the case of communication delays or failures, it will lead to the shutdown of the whole system and even cause disastrous consequences.

Inspired by the existing research work, the contributions of this article in the field of control problems of series–parallel modular converters are as follows.

1) According to the characteristics of modular battery energy storage systems, the application form of droop control is modified to make it suitable for series–parallel expansion and current sharing control of batteries. On this basis, a novel construction method of energy storage system based on battery unit with converters (BUCs) is proposed.
2) For the energy storage system based on BUCs, a two-layer composite control strategy based on improved droop control is proposed. The control strategy not only has high control accuracy but also has good adaptability to communication delays and failures, which is conducive to the safe operation of modular battery energy storage systems. Because of its good adaptability to communication failures, the scheme proposed in this article can adopt low reliability wireless communication, which further improves the scalability of the system.

This article focuses on the control of the series–parallel modular converters. Its control objectives are: 1) to share the output currents of the batteries in each BUC parallel group or series group according to a given ratio and 2) make the total output voltage or current of the energy storage system constant. This article does not discuss the balancing algorithm. The balancing algorithm based on the platform proposed in this article will be left for further research and will be discussed in other papers.

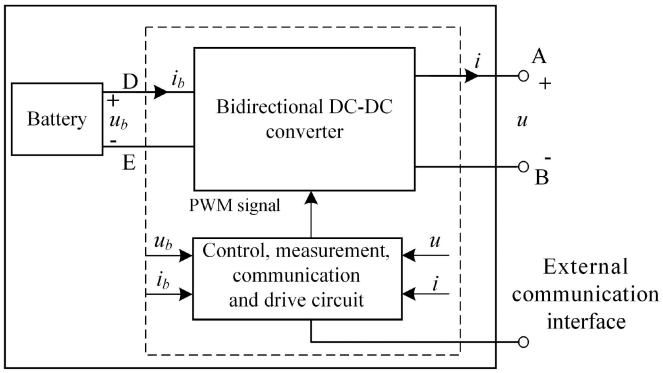


Fig. 1. Schematic diagram of the BUC.

The rest of this article is organized as follows. Section II introduces the concept of BUC proposed in this article. Section III introduces the characteristics of BUC parallel group and series group and the principle of output constant voltage or constant current control of the BUC. Section IV introduces the construction method of energy storage systems based on BUCs. Section V introduces the control strategy of energy storage systems based on BUCs. Section VI presents stability analysis. Section VII is simulation verification. Section VIII is experimental verification. Section IX discusses some key topics. Finally, Section X concludes this article.

## II. Concept of BUC

As shown in Fig. 1, the BUC consists of a battery unit, a bidirectional dc–dc converter and driver circuit, a control circuit, a communication circuit, and a measurement circuit.

The largest solid line box in Fig. 1 represents the BUC, and its internal dotted frame represents the electrical part of the BUC, which is connected to the battery through two power wires. The BUC has an external power output interface and a communication interface. Due to the good adaptability of the control strategy proposed in this article to communication failures, the BUC can adopt low-cost and low-bandwidth wireless communication circuits. If a wireless communication circuit is used, the BUC will only have two power wires connected externally, namely the power interface AB.

The voltage and current relationship (VCR) of the output voltage $u$ and output current $i$ of the BUC mentioned in this article satisfies the droop function shown as follows:

$$\mathrm{u} = \mathrm{b} - \mathrm{Ri}. \tag{1}$$

Equation (1) is a linear function, with current $i$ as the independent variable and voltage $u$ as the function value. In this article, $b$ is referred to as the droop open-circuit voltage, and $R$ is referred to as the droop resistance. If the voltage $u$ is the independent variable and the current $i$ is the function value, another representation of the droop function can be derived from (1), as shown in (2). In (2), $G = 1/R$, which is referred to as droop conductance in this article. The values of $R$ and $G$ are both positive.

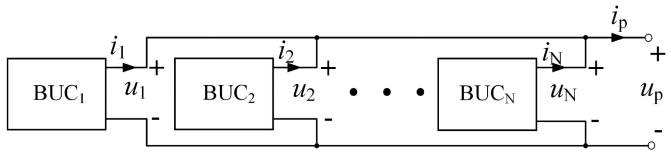


Fig. 2. Parallel BUCs.

$$\mathrm{i} = \mathrm{Gb} - \mathrm{Gu}. \tag{2}$$

## III. Properties of BUCs

### A. Properties of Parallel BUCs

*1) Property of Output VCR of Parallel BUCs:* Fig. 2 shows the parallel BUCs consisting of $N$ BUCs, where $N$ is a positive integer. In the battery energy storage system, the space distance between the batteries is usually close, and the resistance of the wires is usually small. As long as the condition that the droop resistance is far greater than (more than ten times) the wire resistance is met, the wire resistance can be ignored.

The output voltage $u_k$ and output current $i_k$ of these $N$ BUCs satisfy the droop function, as shown in (3), where $k = 1,2,\ldots, N$; $u_k$, $i_k$, $b_k$, and $G_\mathrm{k}$ are respectively the output voltage, output current, droop open-circuit voltage, and droop conductance of the $k$th BUC of parallel BUCs.

$$\mathrm{i}_k = G_k b_k - G_k u_k. \tag{3}$$

It can be proved that the total output voltage $u_p$ and current $i_p$ of parallel BUCs also satisfy the droop function, namely

$$\mathrm{i}_p = G_p b_p - G_p u_p. \tag{4}$$

In (4), $b_p$ and $G_p$ are the droop open-circuit voltage and the droop conductance of parallel BUCs, respectively.

If the voltages of parallel branches are equal, then the following equation can be obtained:

$$\mathrm{u}_k = u_p. \tag{5}$$

When $k = 1,2,\ldots, N$, add all $N$ equations of (3), and substitute (5) into it, then the following equation can be obtained:

$$\sum_{k=1}^{N} \mathrm{i}_k = \sum_{k=1}^{N} G_k b_\mathrm{k} - u_p \sum_{k=1}^{N} G_k. \tag{6}$$

According to Kirchhoff's law, the following equation can be obtained from (6):

$$i_p = \sum_{k=1}^{N} G_k b_\mathrm{k} - u_p \sum_{k=1}^{N} G_k. \tag{7}$$

Let

$$G_p = \sum_{k=1}^{N} G_k \tag{8}$$

$$G_p b_p = \sum_{k=1}^{N} G_k b_k. \tag{9}$$

Substituting (8) and (9) into (7), (4) can be derived, that is, the total output voltage $u_p$ and current $i_p$ of parallel BUCs satisfy the droop function.

*2) Principle of Current Sharing Control of Parallel BUCs:* For all *N* BUCs in parallel, let

$$\mathrm{b}_k = b_p. \tag{10}$$

Combining (3), (5), and (10), the following equation can be obtained:

$$\mathrm{i}_k = G_k b_p - G_k u_p = G_k(b_p - u_p). \tag{11}$$

It can be seen from (11) that $i_k$ is proportional to $G_k$, that is, the output current of each BUC in parallel is proportional to its droop conductance.

The input power $p_{b,k}$ and the output power $p_k$ of the *k*th BUC satisfy

$$\mathrm{u}_p \mathrm{i}_k = \eta_k \mathrm{u}_{b,k} i_{b,k} \tag{12}$$

where $u_{b,k}$ and $i_{b,k}$ are, respectively, the output voltage and current of the battery in the *k*th BUC, and $\eta_k$ is the conversion efficiency of the converter in the *k*th BUC. Under certain conditions, $u_{b,k}$ and $\eta_k$ can be regarded as constant. Therefore, it can be seen from (12) that $i_{b,k}$ and $i_k$ can be approximately regarded as proportional. As mentioned before, $i_k$ and $G_k$ are proportional, so $i_{b,k}$ and $G_k$ can be approximately regarded as proportional. $i_{b,k}$ can be controlled by adjusting $G_k$ so that the battery output currents $i_{b,k}$ of parallel BUCs are shared according to the given ratio.

Use $w_{p,k}$ to represent the ratio of $G_k$. In order to avoid affecting the total droop conductance $G_p$ of parallel BUCs, $G_k$ is not directly adjusted, and instead, $w_{p,k}$ are adjusted by negative feedback according to the error of battery output current, and then calculate $G_k$ as

$$G_k = \frac{w_{p,k}}{\sum_{\mathrm{k}=1}^{N} w_{p,k}} G_p. \tag{13}$$

By using the above method, the accuracy of current sharing of the battery output currents $i_{b,k}$ in parallel BUCs is not affected by the parameters of the circuit components, and its accuracy mainly depends on the measurement accuracy of $i_{b,k}$. Therefore, the current sharing of the battery output currents $i_{b,k}$ in parallel BUCs can achieve pretty high accuracy.

### B. Properties of Series BUCs

*1) Property of Output VCR of Series BUCs:* Fig. 3 shows the series BUCs consisting of *M* BUCs, where *M* is a positive integer.

The output voltage $u_j$ and output current $i_j$ of these *M* BUCs satisfy the droop function, as shown in (14), where $j = 1,2,\ldots, M$; $u_j$, $i_j$, $b_j$, and $R_j$ are, respectively, the output voltage, output current, droop open-circuit voltage, and droop resistance of the *j*th BUC of series BUCs.

$$\mathrm{u}_j = b_j - R_j i_j. \tag{14}$$

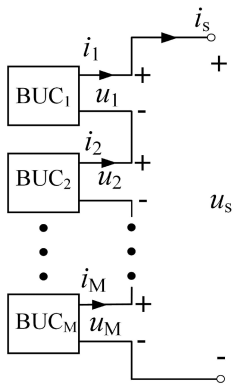


Fig. 3. Series BUCs.

It can be proved that the total output voltage $u_s$ and current $i_s$ of series BUCs also satisfy the droop function, namely

$$\mathrm{u}_s = b_s - R_s i_s. \tag{15}$$

In (15), $b_s$ and $R_s$ are the droop open-circuit voltage and droop resistance of series BUCs respectively.

If the currents of series branches are equal, the following equation can be obtained:

$$\mathrm{i}_j = i_s. \tag{16}$$

When $j = 1,2,\ldots, M$, add all *M* equations of (14), and substitute (16) into it, then the following equation can be obtained:

$$\sum_{j=1}^{M} u_j = \sum_{j=1}^{M} b_j - i_s \sum_{j=1}^{M} R_j. \tag{17}$$

According to Kirchhoff's law, the following equation can be obtained from (17):

$$u_s = \sum_{j=1}^{M} b_j - i_s \sum_{j=1}^{M} R_j. \tag{18}$$

Let

$$\mathrm{b}_s = \sum_{j=1}^{M} b_j \tag{19}$$

$$\mathrm{R}_s = \sum_{j=1}^{M} R_j. \tag{20}$$

Substituting (19) and (20) into (18), (15) can be obtained, that is, the total output voltage $u_s$ and current $i_s$ of series BUCs satisfy the droop function.

*2) Principle of Output Current Sharing of Series BUCs:* For all *M* BUCs in series, let

$$\mathrm{b}_j = \beta R_j \tag{21}$$

where $\beta$ is a constant, that is, $b_j$ is proportional to $R_j$. Combining (14), (16), and (21), the following equation can be obtained:

$$\mathrm{u}_j = \beta R_j - R_j i_s = (\beta - i_s) R_j. \tag{22}$$

According to (22), $u_j$ is proportional to $R_j$, that is, the output voltage of each BUC in series BUCs is proportional to its droop resistance.

The input power $p_{b,j}$ and output power $p_j$ of the $j$th BUC of series BUCs satisfy

$$\mathrm{u}_j \mathrm{i}_s = \eta_j \mathrm{u}_{b,j} i_{b,j} \tag{23}$$

where $u_{b,j}$ and $i_{b,j}$ are, respectively, the output voltage and current of the battery in the $j$th BUC, and $\eta_j$ is the conversion efficiency of the converter in the $j$th BUC. Under certain conditions, $u_{b,j}$ and $\eta_j$ can be regarded as constant. Therefore, it can be seen from (23) that $i_{b,j}$ and $u_j$ can be approximately regarded as proportional. As mentioned before, $u_j$ and $R_j$ are proportional, so $i_{b,j}$ and $R_j$ can be approximately regarded as proportional. Hence, $i_{b,j}$ can be controlled by adjusting $R_j$ so that the battery output currents $i_{b,j}$ of series BUCs are shared according to the given ratio.

Use $w_{s,j}$ to represent the ratio of $R_j$. In order to avoid affecting the total droop resistance $R_s$ of series BUCs, $R_j$ is not directly adjusted, and instead, $w_{s,j}$ is adjusted by negative feedback according to the error of battery output current, and then $R_j$ is calculated by

$$R_j = \frac{w_{s,j}}{\sum_{j=1}^{M} w_{s,j}} R_s. \tag{24}$$

In addition, (21) shows that $b_j$ is proportional to $R_j$. Therefore, $w_{s,j}$ also represent the ratio of $b_j$. Combined with (19), the relationship between the droop open-circuit voltage $b_j$ of each BUC of series BUCs and the droop open-circuit voltage $b_s$ of the series BUCs can be obtained

$$b_j = \frac{w_{s,j}}{\sum_{j=1}^{M} w_{s,j}} b_s. \tag{25}$$

### C. Principle of Output Constant Voltage or Constant Current Control of the BUC

As mentioned in Section II, the output voltage and current of a BUC are referred to as $u$ and $i$, respectively, and the equivalent resistance of the load connected to the BUC is referred to as $R_L$, the following equation can be obtained from Ohm's law:

$$u = R_L i. \tag{26}$$

From (1) and (26), the following equations can be obtained:

$$u = \frac{b}{1 + \frac{R}{R_L}} \tag{27}$$

$$i = \frac{b}{R + R_L}. \tag{28}$$

According to (27), when the droop resistance $R$ and the load resistance $R_L$ of the BUC are constant, the output voltage $u$ of the BUC is controlled by the droop open-circuit voltage $b$, and by detecting BUC output voltage $u$, and then adjusting $b$ by negative feedback according to the output voltage error, the constant output voltage can be achieved. Similarly, it can be seen from (28), by detecting BUC output current $i$, and then adjusting $b$ by negative feedback according to the output current error, the constant output current can be achieved.

## IV. Construction Method of Energy Storage System Based on BUCs

### A. Construction Method

The energy storage system based on BUCs can be constructed in one of the following ways or a combination of several ways:

*Way 1:* Connect the outputs of $N$ BUCs in parallel to form a group of parallel BUCs, where $N$ is a positive integer.

*Way 2:* Connect the outputs of $M$ BUCs in series to form a group of series BUCs, where $M$ is a positive integer.

*Way 3:* Since the output voltage and current of the group of parallel BUCs or the group of series BUCs also satisfy the droop function, the group of parallel BUCs or the group of series BUCs can be equivalent to a BUC. The equivalent BUC can be connected in series or in parallel with other BUCs according to Way 1 or Way 2 to form a larger group of parallel BUCs or a larger group of series BUCs.

### B. Three Concepts About the Construction Method

To facilitate the understanding of the construction method proposed in this article, the following three concepts are defined.

*Definition of the concept of an entity BUC:* An entity BUC refers to a single BUC that physically exists. It is not an equivalent BUC, and an entity BUC contains only one BUC within itself.

*Definition of the concept of an equivalent BUC:* An equivalent BUC refers to an energy storage system composed of multiple entity BUCs, constructed based on the BUC-based energy storage system method proposed in this article. The total output voltage and current of this energy storage system satisfy the droop function, allowing it to be equivalently regarded as a single BUC, known as an equivalent BUC. An equivalent BUC contains multiple entity BUCs within it.

*Definition of the concept of BUC level:* In a BUC-based energy storage system, if the total output voltage and current of the entire energy storage system satisfy the droop function, it can be equivalently considered as a single BUC, which is defined as a level-0 BUC. A level-0 BUC may be either a series group or a parallel group of BUCs. The entity BUCs or equivalent BUCs that directly form the level-0 BUC through series or parallel connections are referred to as level-1 BUCs. By analogy, a level-n equivalent BUC may be a series or parallel group of BUCs, and the entity or equivalent BUCs that directly form the level-n BUC through series or parallel connections are referred to as level-(n+1) BUCs, where n is 0 or a positive integer. In a BUC-based energy storage system, a certain BUC consists entirely of entity BUCs without any equivalent BUCs, and its BUC level is denoted as h-1. The maximum value of h among all such BUCs is defined as H, which represents the highest BUC level in the energy storage system, as illustrated in the Fig. 4, and the highest BUC level is level-3.

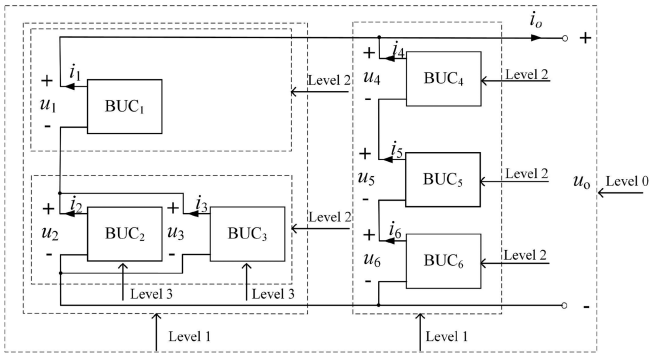


Fig. 4. Concept of the BUC level.

### C. Characteristics of the Construction Method

Compared with existing technologies, the construction method proposed in this article has the following characteristics.

1) The proposed BUC can be connected in both parallel and series configurations by using the same hardware and a unified control strategy. In contrast, existing technologies only allow for either series or parallel connections. If both series and parallel connections are required simultaneously, different methods and control strategies must be employed.
2) The most distinctive feature of the proposed construction method is equivalent nesting, which means that an equivalent BUC can be regarded as a single BUC and then further connected in parallel or series with other BUCs to form an energy storage system.
3) The proposed construction method and control strategy do not require the number of BUCs in each series or parallel group to be equal. The number of BUCs can be any positive integer.
4) The proposed construction method is highly flexible, allowing for the construction of a BUC-based energy storage system with arbitrary connection configurations. The only requirement is that the operating voltage and current ranges of the output terminals of all BUCs must be compatible.
5) The proposed construction method is also highly convenient. To integrate a BUC into an energy storage system, one only needs to connect two power wires to the output terminals of the BUC.

## V. Control Strategy of Energy Storage System Based on BUCs

For the control of energy storage systems based on BUCs, this article focuses on the key problem: how to make many series and parallel BUCs work together stably, and achieve the following control objectives: 1) Make the output current of batteries in each BUC parallel group or series group shared according to the given ratio. 2) Make the total output voltage or total output current of the energy storage system constant. In order to achieve the above control objectives, this article proposes a two-layer control strategy based on improved droop control, including the lower control strategy and the upper control strategy. The lower control strategy is implemented locally on each entity BUC (not equivalent to BUC) without communication between BUCs so that the output voltage and current of each entity BUC satisfy the droop function. The lower control strategy can work without communication, so it has high stability. However, because droop control is easily affected by circuit parameters and other factors, the control accuracy of the system is low when there is only the lower control strategy. With low-bandwidth communication, the upper control strategy measures the controlled variables such as battery currents and the total output voltage, and adjusts the two parameters of the droop function of each BUC by negative feedback according to the errors of the controlled variables, so the control accuracy of the system is further improved. When communication fails, the upper control strategy automatically and smoothly exits, and the system is controlled by the lower control strategy. Depending on the time length of communication failure, the control accuracy maybe decline to some extent but the system is still stable. When the communication is normal, the upper control strategy automatically and smoothly takes effect, and the system is controlled by the two-layer control strategy, which has high control accuracy.

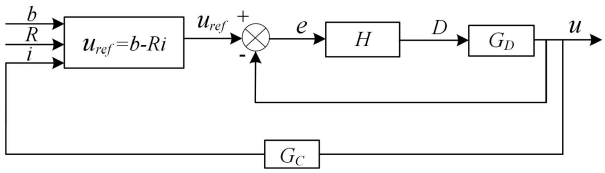


Fig. 5. Control diagram of the lower control strategy.

### A. Lower Control Strategy

The lower control strategy is implemented locally on each entity BUC so that the output voltage $u$ and output current $i$ of each entity BUC meet the droop function shown in (1). The lower control strategy is shown in Fig. 5. In Fig. 5, $u$ represents the output voltage of the BUC; $u_{\rm ref}$ represents the given value of output voltage; $e$ indicates the voltage error; $D$ represents the duty cycle of the dc–dc; $i$ represents the output current of the BUC; $G_D$ represents the transfer function of the dc–dc; $H$ represents the transfer function of the compensator; $G_C$ represents the transfer function between the $u$ and $i$. The output voltage and current satisfy the droop function through the voltage and current double closed-loop control. The details are as follows: the current outer loop detects the output current and uses the droop function to calculate the given value of the output voltage, which is assigned to the voltage inner loop. The voltage inner loop adopts constant voltage control.

### B. Upper Control Strategy

The upper control strategy Fig. 6, can improve the accuracy of output current sharing control of batteries according to the given ratio and make the total output voltage or current of the energy

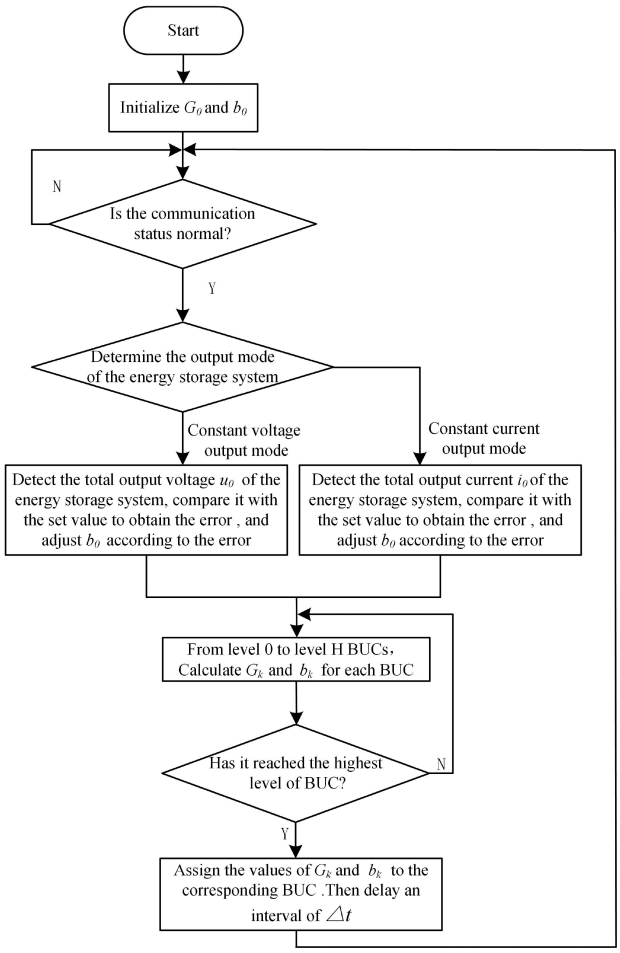


Fig. 6. Flowchart of the upper control strategy.

storage system constant. The algorithm of the upper control strategy is as follows.

*Step 1:* Regard the whole energy storage system based on BUCs as an equivalent BUC, and its output meets the droop function. Its droop resistance is $R_0$, droop conductance is $G_0 = 1/R_0$, and droop open-circuit voltage is $b_0$. Give droop conductance $G_0$ and droop open-circuit voltage $b_0$ appropriate initial values.

*Step 2:* Judge whether the communication between BUCs is normal. If it is normal, go to step 3; if not, go to step 2.

*Step 3:* If the energy storage system is in constant voltage output mode, detect the total output voltage $u_0$ of the energy storage system, and adjust $b_0$ by negative feedback according to the error of the voltage $u_0$ to obtain a new value of $b_0$. If the energy storage system is in constant current output mode, the total output current $i_0$ is detected, and $b_0$ is adjusted by negative feedback according to the error of current $i_0$ to obtain a new value of $b_0$.

*Step 4:* Starting from the droop conductance $G_0$ and droop open-circuit voltage $b_0$ of the energy storage system, calculate the droop conductance (or droop resistance) and droop open-circuit voltage of each BUC in turn. For the group of parallel BUCs, (10) and (13) are used for calculation. For the group of series BUCs, (24) and (25) are used for calculation. Before calculation, the negative feedback adjustment of $w_{p,k}$ or $w_{s,j}$ shall be carried out according to the error of battery output current to obtain the latest value of $w_{p,k}$ or $w_{s,j}$, which shall be substituted into the formula for calculation.

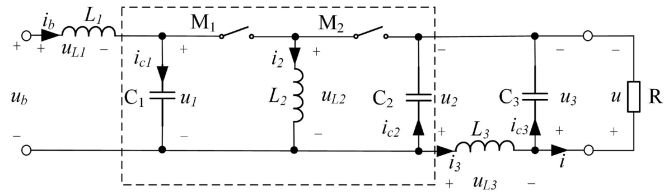


Fig. 7. Schematic of the DC–DC main circuit.

*Step 5:* Assign the droop open-circuit voltage and droop conductance (or droop resistance) of each BUC calculated in step 4 to each BUC. After an appropriate interval $\triangle t$, then jump to step2 to continue the algorithm.

## VI. Stability Analysis

### A. Small-Signal Analysis and Stability of a Single BUC

The stability of a single BUC is analyzed using the small-signal analysis method. The dc–dc main circuit of the proposed BUC is shown in Fig. 7, where the dashed box represents the circuit of a conventional synchronous rectified buck–boost converter. To further reduce fluctuations in the input and output currents, a small-capacity inductor is added at the input of the conventional buck–boost converter, while an *LC* filter, composed of a small-capacity inductor and capacitor, is added at the output. The proposed BUC can also adopt other types of bidirectional dc–dc circuits. However, using the circuit shown in Fig. 7 offers the following advantages. It requires only two switching transistors, reducing component costs. The output voltage can be both stepped up and stepped down, and this allows for a wider range of battery output current ratios in series BUCs. The output current ripple is small, contributing to system stability. The input current ripple is also reduced to a reasonable range, which benefits battery lifespan and safe operation.

Using the average current method, the state equations of the circuit shown in Fig. 7 at the steady-state operating point can be formulated as follows:

$$\mathrm{L}_1 \frac{di_b}{dt} = u_b - u_1 \tag{29}$$

$$\mathrm{L}_2 \frac{di_2}{dt} = u_1 D - u_2 + u_2 D \tag{30}$$

$$\mathrm{L}_3 \frac{di_3}{dt} = u_2 - u_3 \tag{31}$$

$$\mathrm{C}_1 \frac{du_1}{dt} = i_1 - i_2 D \tag{32}$$

$$\mathrm{C}_2 \frac{du_2}{dt} = i_2 - i_2 D - i_3 \tag{33}$$

$$\mathrm{C}_3 \frac{du_3}{dt} = i_3 - \frac{u_3}{R}. \tag{34}$$

From the abovementioned equations, the small-signal state equations can be derived as follows:

$$\mathrm{L}_1\frac{d\tilde{i}_b}{dt} = -\tilde{u}_1 \tag{35}$$

$$\mathrm{L}_2\frac{d\tilde{i}_2}{dt} = u_1\tilde{D} + \tilde{u}_1 D - \tilde{u}_2 + u_2\tilde{D} + \tilde{u}_2 D \tag{36}$$

$$\mathrm{L}_3\frac{d\tilde{i}_3}{dt} = \tilde{u}_2 - \tilde{u}_3 \tag{37}$$

$$\mathrm{C}_1\frac{d\tilde{u}_1}{dt} = \tilde{i}_1 - i_2\tilde{D} - \tilde{i}_2 D \tag{38}$$

$$\mathrm{C}_2\frac{d\tilde{u}_2}{dt} = \tilde{i}_2 - i_2\tilde{D} - \tilde{i}_2 D - \tilde{i}_3 \tag{39}$$

$$\mathrm{C}_3\frac{d\tilde{u}_3}{dt} = \tilde{i}_3 - \frac{\tilde{u}_3}{R}. \tag{40}$$

By applying the Laplace transform to the above small-signal equations and solving the Laplace equations, the transfer function $G_D$ between the duty cycle $D(s)$ and the output voltage $U_3(s)$ can be obtained as follows:

$$G_D = \frac{B_3S^3 + B_2S^2 + B_1S + B_0}{A_6S^6 + A_5S^5 + A_4S^4 + A_3S^3 + A_2S^2 + A_1S + A_0}. \tag{41}$$

In (41), the coefficients are represented as follows:

$$\begin{aligned}
B_0 &= -R(Du_1 + D\mathrm{u}_2 - u_1 - u_2)\\
B_1 &= -RL_2i_2 - RDL_1i_2\\
B_2 &= -R(-C_1L_1u_1 - C_1L_1u_2 + C_1DL_1u_1 + C_1DL_1u_2)\\
B_3 &= -RC_1L_1L_2i_2\\
A_0 &= R + D^2R - 2DR\\
A_1 &= L_2 + L_3 - 2DL_3 + D^2L_1 + D^2L_3\\
A_2 &= C_1L_1R + C_2L_2R + C_3L_2R + C_3L_3R - 2C_1DL_1R\\
&\quad - 2C_3DL_3R + C_1D^2L_1R + C_2D^2L_1R + C_3D^2L_1R\\
&\quad + C_3D^2L_3R\\
A_3 &= C_1L_1L_2 + C_1L_1L_3 + C_2L_2L_3 - 2C_1DL_1L_3\\
&\quad + C_1D^2L_1L_3 + C_2D^2L_1L_3\\
A_4 &= C_1C_2L_1L_2R + C_1C_3L_1L_2R + C_1C_3L_1L_3R\\
&\quad + C_2C_3L_2L_3R + C_1C_3D^2L_1L_3R + C_2C_3D^2L_1L_3R\\
&\quad - 2C_1C_3DL_1L_3R\\
A_5 &= C_1C_2L_1L_2L_3\\
A_6 &= C_1C_2C_3L_1L_2L_3R.
\end{aligned}$$

Let the transfer function of the voltage loop compensator be

$$\mathrm{H} = \frac{D(s)}{e(s)} = Kp + \frac{Ki}{s}. \tag{42}$$

The closed-loop transfer function of the voltage loop $Gv$ can be obtained as

$$Gv = \frac{U(s)}{U_{ref}(s)} = \frac{HG_D}{1 + HG_D}. \tag{43}$$

The open-loop transfer function $G_D$ is a sixth-order system. By applying PI compensator, as shown in (42), all poles of the closed-loop transfer function $Gv$ can be shifted to the left-half plane, thereby satisfying stability requirements. In addition, since the values of $L_1$, $C_1$, $L_3$, and $C_3$ are much smaller than those of $L_2$ and $C_2$, $G_D$ can be approximated as a second-order system when high precision is not required. However, because the transfer function $G_D$ does not account for line resistance, there are some slight discrepancies between it and the actual system. Furthermore, noise exists in practical systems. Experimental results indicate that adding an appropriate derivative control to the PI controller reduces output voltage fluctuations.

The small-signal model can be used to analyze the small-signal stability of dc–dc converters, serving as the foundation for large-signal stability analysis. Although the transfer function $G_D$ is no longer valid under large-signal disturbances, the positive correlation between the duty cycle and output voltage can still be used to demonstrate the system's stability under large-signal conditions.

### B. System Stability Analysis

In the previous section, the stability of the voltage loop of a single BUC was analyzed based on the small-signal analysis method. This section attempts to analyze the stability of the BUC-based energy storage system. However, when applying the small-signal analysis method to system-level stability, the following three challenges arise.

1) *Complexity of system-level analysis:* Even for a simple parallel system with only three BUCs, deriving the system's transfer function matrix using small-signal analysis becomes highly complex. The variables are strongly coupled, making it impractical to proceed with this approach.
2) *Independence from specific dc–dc converters:* The proposed energy storage system construction method is not limited to a specific type of DC-DC converter. Therefore, system-level stability analysis does not rely on the transfer function of a particular converter. Instead, the essential characteristics of dc–dc converters applicable to this system can be abstracted, and a generalized dc–dc converter model can be used for system-level analysis.
3) *Limitations of small-signal analysis:* The small-signal analysis method only assesses small-signal stability, which serves as the foundation for large-signal stability. However, it does not directly prove the system's large-signal stability.

Inspired by the above issues, this article aims to analyze and verify system stability without establishing an exact model of the dc–dc converter. To theoretically prove system stability, an appropriate mathematical framework is required. The Lyapunov virtual energy function provides a suitable mathematical tool for this purpose. The following section attempts to use Lyapunov's

second method to prove the system-level stability of a parallel BUC group.

*1) Equilibrium State and Coordinate Transformation:* Assume that there are a total of $N$ BUCs in the system. Their output voltages and currents are $u_k$ and $i_k$, respectively. The load resistance of the system is $R_L$. Considering the internal resistance of the line, according to the substitution theorem and the superposition theorem, we can obtain

$$\mathrm{i}_k = \sum_{j=1}^{N} \mathrm{Y}_{k,j} u_j. \tag{44}$$

In the above equation, $Y_{k,j}$ is a constant coefficient related to the line resistance and load resistance, where $k = 1,2,\ldots,N; j = 1,2,\ldots,N$.

When the system reaches equilibrium, we have

$$\mathrm{u}_k = u_{ref,k} \tag{45}$$

where $u_{\mathrm{ref},k}$ is the reference voltage for the inner voltage control loop of the dc–dc converter in the $k$th BUC. Based on the current outer loop control strategy, we derive the following equation:

$$u_{\mathrm{ref},k} = b_k - R_k i_k. \tag{46}$$

Using (44)–(46), and applying the linear circuit theory, a unique set of solutions $u_{e,k}$ can be obtained, representing the system's equilibrium state. Let $u_{e,k}$ and $i_{e,k}$ denote the equilibrium output voltage and current of each BUC, respectively. Taking the equilibrium state as the coordinate origin, the following coordinate transformation can be performed:

$$\mathrm{u}_k = u_{\mathrm{e},k} + \Delta \mathrm{u}_k \tag{47}$$

$$\mathrm{i}_k = i_{e,k} + \Delta \mathrm{i}_k. \tag{48}$$

In the above equation, $\Delta u_k$ and $\Delta i_k$ represent the deviations of the current voltage and current from the equilibrium state, respectively. $u_{ref,k}$ can also be expressed as

$$\mathrm{u}_{\mathrm{ref},k} = u_{\mathrm{eref},k} + \Delta u_{\mathrm{ref},k}. \tag{49}$$

In (49), $u_{\mathrm{eref},k}$ is the reference value of the voltage inner loop of the dc–dc converter in the $k$th BUC at equilibrium, and $\Delta u_{\mathrm{ref},k}$ represents the deviation of the current voltage reference value from the equilibrium state. Based on the control strategy of the outer current loop, the following equation can be obtained:

$$u_{\mathrm{eref},k} = b_k - R_k i_{e,k}. \tag{50}$$

From (46), (48), (49), and (50), it can be derived that

$$\Delta u_{\mathrm{ref},k} = -R_k \Delta i_k. \tag{51}$$

*2) DC–DC Converter Model for System Stability Analysis:* When conducting a system stability analysis, the dc–dc converter is assumed to have the following two characteristics.

1) $\Delta u_k(0)$ and $\Delta u_{\mathrm{ref},k}$ represent the initial value and the reference value of the dc–dc output voltage, respectively. It is assumed that after a finite period, the dc–dc output voltage $\Delta u_k$ can stabilize from $\Delta u_k(0)$to $\Delta u_{\mathrm{ref},k}$.
2) $\Delta u_k$ and $\Delta u_{\mathrm{ref},k}$ represent the dc–dc output voltage and its reference value at a certain moment, respectively. It is assumed that when $\Delta u_{\mathrm{ref},k} > \Delta u_k$, then $\mathrm{d}(\Delta u_k)/\mathrm{d}t > 0$; when $\Delta u_{\mathrm{ref},k} < \Delta u_k$, then $\mathrm{d}(\Delta u_k)/\mathrm{d}t < 0$. In other words, when the voltage reference value is greater than the current voltage, the voltage increases; when the voltage reference value is smaller than the current voltage, the voltage decreases.

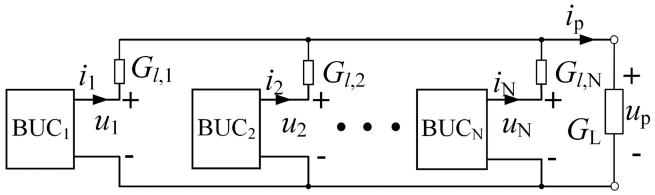


Fig. 8. Parallel BUCs with resistors.

A dc–dc converter that remains stable under large-signal conditions can be considered to satisfy the above-mentioned two conditions.

*3) Stability Analysis of the BUC Parallel Group:* The BUC parallel group is shown in Fig. 8. Based on linear circuit theory, the following equation can be obtained:

$$\Delta \mathrm{i}_k = G_{l,k} \left( \Delta u_k - \frac{\sum_{k=1}^{N} G_{l,k} \Delta u_k}{G_L + \sum_{k=1}^{N} G_{l,k}} \right). \tag{52}$$

In the above-mentioned equation, $G_{l,k}$ represents the conductance of the output line resistance of the $k$th BUC, and $G_L$ represents the conductance of the load resistor.

By rearranging (52), we get

$$\Delta \mathrm{i}_k = G_{l,k} \frac{\sum_{k=1}^{N} G_{l,k}}{G_L + \sum_{k=1}^{N} G_{l,k}} \left( \left( \Delta u_k - \frac{\sum_{k=1}^{N} G_{l,k} \Delta u_k}{\sum_{k=1}^{N} G_{l,k}} \right) + \frac{G_L}{\sum_{k=1}^{N} G_{l,k}} \Delta u_k \right). \tag{53}$$

Let

$$\mathrm{u}_{\mathrm{WA}} = \frac{\sum_{k=1}^{N} G_{l,k} \Delta u_k}{\sum_{k=1}^{N} G_{l,k}} \tag{54}$$

$$\varepsilon = \frac{G_L}{\sum_{k=1}^{N} G_{l,k}}. \tag{55}$$

Thus, (53) can be rewritten as

$$\Delta \mathrm{i}_k = G_{l,k} \frac{\sum_{k=1}^{N} G_{l,k}}{G_L + \sum_{k=1}^{N} G_{l,k}} ((\Delta u_k - u_{\mathrm{WA}}) + \varepsilon \Delta u_k). \tag{56}$$

In (56), $u_{\mathrm{WA}}$ is the weighted average of $\Delta u_k$ with $G_{l,k}$ as the weighting coefficient. Since the line resistance is very small, $G_{l,k}$ is a very large value, and in most cases, $G_{l,k}>>G_L$, so $\varepsilon$ *is a very small value.*

From (51) and (56), we get

$$\Delta \mathrm{u}_{\mathrm{ref},k} = -R_k G_{l,k} \frac{\sum_{k=1}^{N} G_{l,k}}{G_L + \sum_{k=1}^{N} G_{l,k}} ((\Delta u_k - u_{\mathrm{WA}}) + \varepsilon \Delta u_k). \tag{57}$$

From (57), we can see that the dynamic change pattern of $\Delta u_k$ in the BUC parallel group is as follows: Since $\varepsilon$ is a very small value, when $\Delta u_k$ is not equal to $u_{\mathrm{WA}}$, the value of $\Delta u_{\mathrm{ref},k}$ is determined by $\Delta u_k$-$u_{WA}$. At this time, when $\Delta u_k > u_{\mathrm{WA}}$, $\Delta u_{\mathrm{ref},k}<0$, which makes $\Delta u_k$ decrease, and when $\Delta u_{k<} u_{\mathrm{WA}}$, $\Delta u_{\mathrm{ref},k}>0$, which makes $\Delta u_k$ increase. Ultimately, $\Delta u_k$ approaches $u_{\mathrm{WA}}$, and when $\Delta u_k$-$u_{\mathrm{WA}}$ approaches 0, the value of $\Delta u_{\mathrm{ref},k}$ is determined by $\varepsilon \Delta u_k$. When $\Delta u_k>0$, $\Delta u_{\mathrm{ref},k}<0$, which makes $\Delta u_k$ decrease; when $\Delta u_{k<}0$, $\Delta u_{\mathrm{ref},k}>0$, which makes $\Delta u_k$ increase. Eventually, all $\Delta u_k$ approach 0, thus reaching the equilibrium state.

Based on the insights from the above dynamic behavior, a Lyapunov function can be constructed as follows:

$$V(\Delta u_k) = \sum_{k=1}^{N} ((\Delta u_k - u_{\mathrm{WA}})^2 + \varepsilon \Delta {u_k}^2). \tag{58}$$

Since $\varepsilon>0$, it is evident that at equilibrium, $V(\Delta u_k) = 0$, and in a nonequilibrium state, $V(\Delta u_k)>0$. Taking the time derivative of $V(\Delta u_k)$ gives

$$\frac{dV}{dt} = 2\sum_{k=1}^{N} \left( (\Delta u_k - u_{\mathrm{WA}} + \varepsilon \Delta u_k) \frac{d(\Delta u_k)}{dt} \right) - 2\frac{du_{\mathrm{WA}}}{dt} \sum_{k=1}^{N} (\Delta u_k - u_{\mathrm{WA}}). \tag{59}$$

When the line resistance of the wires in each parallel branch is equal, the following equation can be derived:

$$\sum_{k=1}^{N} (\Delta u_k - u_{\mathrm{WA}}) = 0. \tag{60}$$

$dV/dt$ can be changed to

$$\frac{dV}{dt} = 2\sum_{k=1}^{N} \left( (\Delta u_k - u_{\mathrm{WA}} + \varepsilon \Delta u_k) \frac{d(\Delta u_k)}{dt} \right). \tag{61}$$

The proof that $dV/dt \leq 0$ is presented as follows, considering the three cases.

*Case a:* When $\Delta u_k$-$u_{\mathrm{WA}}+\varepsilon \Delta u_k>0$, it is only necessary to prove that $\Delta u_{\mathrm{ref},k}<\Delta u_k$, which leads to $d(\Delta u_k)/dt<0$. Consequently, all terms of $dV/dt$ are negative, resulting in $dV/dt<0$. To prove $\Delta u_{\mathrm{ref},k}<\Delta u_k$, we consider the following two subcases.

*Case a.1:* When $\Delta u_k$-$u_{\mathrm{WA}} \leq 0$, since $\Delta u_k$-$u_{\mathrm{WA}}+\varepsilon \Delta u_k>0$, it follows that $\Delta u_k>0$ because $\Delta u_k$-$u_{\mathrm{WA}}+\varepsilon \Delta u_k>0$, from (57), we know that $\Delta u_{\mathrm{ref},k}<0$, thus proving $\Delta u_{\mathrm{ref},k}<\Delta u_k$.

*Case a.2:* When $\Delta u_k$-$u_{\mathrm{WA}}>0$, from (57), the inequality $\Delta u_{\mathrm{ref},k}<\Delta u_k$ can be rewritten as

$$-R_k G_{l,k} \frac{\sum_{k=1}^{N} G_{l,k}}{G_L + \sum_{k=1}^{N} G_{l,k}} ((\Delta u_k - u_{\mathrm{WA}}) + \varepsilon \Delta u_k) < \Delta u_k. \tag{62}$$

The above inequality can be transformed into

$$u_{\mathrm{WA}} < \left( 1 + \varepsilon + \frac{G_L + \sum_{k=1}^{N} G_{l,k}}{R_k G_{l,k} \sum_{k=1}^{N} G_{l,k}} \right) \Delta u_k. \tag{63}$$

When the load resistance $R_L$ and the droop resistance $R_k$ are much greater than the line resistance $R_{l,\mathrm{k}} = 1/G_{l,k}$, the above inequality can be simplified to $u_{\mathrm{WA}}<\Delta u_k$. This is the premise of Case a.2, thus proving this situation.

*Case b:* When $\Delta u_k$-$u_{\mathrm{WA}}+\varepsilon \Delta u_k<0$, it is only necessary to prove that $\Delta u_{\mathrm{ref},k}>\Delta u_k$, which leads to $d(\Delta u_k)/dt>0$. Consequently, all terms of $dV/dt$ are negative, resulting in $dV/dt<0$. Since Case b is the dual of Case a, its proof follows a similar process, which is omitted here for brevity.

*Case c:* When $\Delta u_k$-$u_{\mathrm{WA}}+\varepsilon \Delta u_k = 0$, this term in the expression for $dV/dt$ becomes zero, and the sign of $dV/dt$ is determined by other nonzero terms.

By synthesizing these three cases, we obtain $dV/dt \leq 0$. Moreover, it can be shown that if $dV/dt = 0$, then all $\Delta u_k = 0$, indicating that the system is in equilibrium.

In conclusion: In equilibrium: $V(\Delta u_k) = 0$ and $dV/dt = 0$. In a nonequilibrium state: $V(\Delta u_k)>0$ and $dV/dt<0$. As $\Delta u_k$ tends to infinity, $V(\Delta u_k)$ also tends to infinity. Thus, according to Lyapunov's second method, the BUC parallel group, under the proposed lower control strategy, is a globally asymptotically stable system.

In addition, the small-signal analysis method in the previous section only proved the stability of the voltage loop of a single BUC, without proving the stability of its current loop. Based on the conclusions of this section, a single BUC can be regarded as a special case of the BUC parallel group with only one unit. Therefore, a single BUC is also a globally asymptotically stable system.

## VII. Simulation Verification

As shown in Fig. 9, a simulation model of the energy storage system consisting of nine BUCs was constructed on the MATLAB Simulink Simscape platform. The discharging experiments, charging experiments, and communication failure experiments were conducted on this simulation model. The schematic diagram of the dc–dc main circuit contained in the BUC is shown in Fig. 7, with circuit component parameters listed in Table I. Fig. 10 shows the simulation diagram of a single BUC. A 12 V 7 Ah lead-acid battery is used as the battery. To better simulate the actual circuit, the internal resistance of the components is considered, and a random deviation of about 10% is added to the component parameters. Fig. 11 shows the control

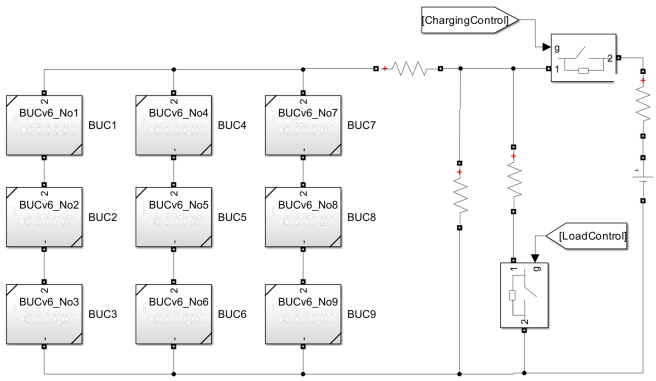


Fig. 9. System simulation diagram.

TABLE I
COMPONENT PARAMETERS OF THE DC–DC CONVERTER

| Designator | Parameters |
|---|---|
| $L_1$ | 47μH |
| $L_2$ | 500μH |
| $L_3$ | 10μH |
| $C_1$ | 220μF |
| $C_2$ | 470μF |
| $C_3$ | 100μF |

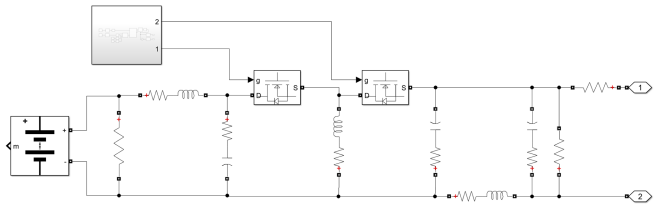

Fig. 10. Simulation diagram of a single BUC.

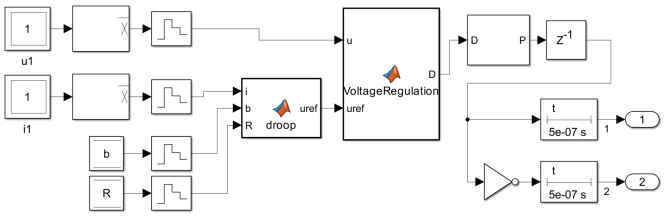


Fig. 11. Control diagram of a single BUC.

diagram of a single BUC. To better simulate the scenario where a microcontroller controls the actual circuit, a fixed-step discrete control method is adopted. The lower control strategy shown in Fig. 5 is implemented mainly through two MATLAB functions in the form of code. In addition, a MATLAB function is used to implement the upper control strategy in the entire simulation system.

### A. Discharging Simulation Experiment

The energy storage system was discharged at a constant voltage, with the total output voltage set to 36 V and the load resistance at 12 Ω. The output currents of the batteries in the nine BUCs were set to be shared in two ratios, called mode 1 and mode 2. Data for both modes are given in Table II. In Table II, $\boldsymbol{i_b}$ represents the matrix of battery output currents, defined as in (64). The $\boldsymbol{i_{b\_ratio\_ref}}$ represents the matrix of reference sharing ratios of the battery output currents, with elements ordered similarly to $\boldsymbol{i_b}$.

TABLE II
DISCHARGING SIMULATION EXPERIMENT

| | $\boldsymbol{i_{b\_ratio\_ref}}$ | $\boldsymbol{i_b}$/A | Current sharing error | Total Output Voltage (V) | Total Output Voltage Error |
|---|---|---|---|---|---|
| Mode 1 | 1 1 1<br>1 1 1<br>1 1 1 | 0.957 0.968 0.961<br>0.963 0.946 0.951<br>0.958 0.968 0.967 | 0.63% | 36.00 | 0% |
| Mode 2 | 2 3 1<br>1 1 1<br>1 1 1 | 1.433 2.168 0.723<br>0.733 0.719 0.715<br>0.731 0.726 0.733 | 0.78% | 36.00 | 0% |

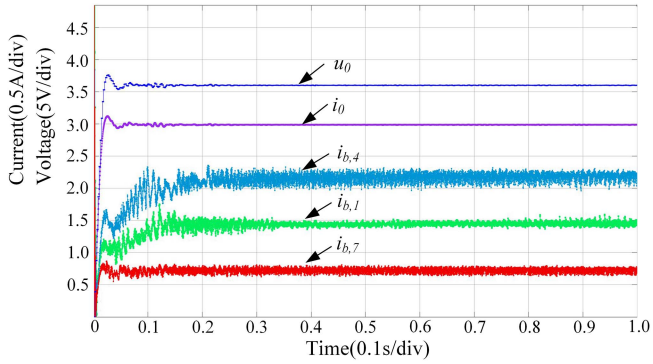


Fig. 12. Discharging simulation experiment.

$$i_b = \begin{bmatrix} i_{b,1} & i_{b,4} & i_{b,7} \\ i_{b,2} & i_{b,5} & i_{b,8} \\ i_{b,3} & i_{b,6} & i_{b,9} \end{bmatrix}. \tag{64}$$

The current sharing error in Table II is calculated as follows: Let $e_k$ be the output current sharing error for the $k$th battery. Based on the set sharing ratios of the battery output currents and the sum of the measured output current of every battery, the target output current $i_{b\_\mathrm{ref},k}$ for the $k$th battery can be calculated. The measured output current of the $k$th battery is $i_{bk}$. Thus, the current sharing error $e_k$ for the $k$th battery is given by

$$\mathrm{e}_k = ((i_{b,k} - i_{\mathrm{bref},k})/i_{\mathrm{bref},k}) \times 100\%. \tag{65}$$

The battery output current sharing error of the whole system is taken as the average of the absolute values of all $e_k$.

Fig. 12 shows the discharging simulation waveforms for mode 2, which is similar to mode 1. From top to bottom, the five waveforms in Fig. 12 are the total output voltage $u_o$, the total output current $i_0$, the battery output current $i_{b,4}$ of the fourth BUC, the battery output current $i_{b,1}$ of the first BUC, and the battery output current $i_{b,7}$ of the seventh BUC. For better display, $u_o$ is multiplied by 0.1. The total output voltage $u_o$ and total output current $i_0$ reach steady state at approximately 0.06 s, while the output currents of the individual batteries reach steady

TABLE III
CHARGING SIMULATION EXPERIMENT

| | $i_{b\_rati\text{-}o\_ref}$ | $i_b$/A | Current sharing error | Total output current (A) | Total output current error |
|---|---|---|---|---|---|
| Mode 1 | 1 1 1 | -0.870 -0.870 -0.868 | | | |
| | 1 1 1 | -0.867 -0.872 -0.873 | 0.18% | -3.000 | 0% |
| | 1 1 1 | -0.869 -0.868 -0.866 | | | |
| Mode 2 | 2 3 1 | -1.300 -1.950 -0.649 | | | |
| | 1 1 1 | -0.650 -0.645 -0.651 | 0.30% | -3.000 | 0% |
| | 1 1 1 | -0.651 -0.647 -0.645 | | | |

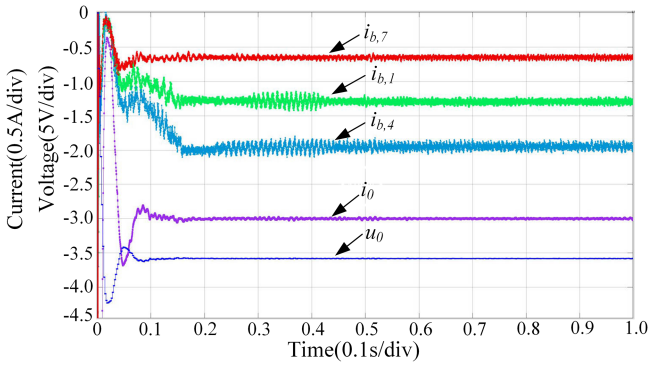


Fig. 13. Charging simulation experiment.

state at around 0.15 s. After reaching steady state, the average total output voltage $u_o$ is 36.00 V with zero error, and the voltage ripple amplitude percentage is 0.24%. The average total output current $i_0$ is 2.986 A, with a current ripple amplitude percentage of 0.29%.The current sharing errors of the entire system are no more than 0.78%, with the average percentage of battery output current ripple amplitude being 11.8%, the minimum value 7.6%, and the maximum value 15.6%. Under the effect of the input filter, the ripple at the pulsewidth modulation (PWM) switching frequency is reduced to about 0.04 A, which is negligible. The main component of the battery output current ripple, with a period of milliseconds, cannot be completely eliminated. In the proposed energy storage system, the battery output current is an internal variable, so its ripple does not affect the external output performance of the system. In addition, since the relationship between the state of charge (SOC) and the battery output current is integral, and the control accuracy of the average battery output current is pretty high, approximately 0.78%, the ripple of the battery output current has a negligible effect on SOC balancing.

### B. Charging Simulation Experiment

The energy storage system was charged at a constant current, with the total output current set to −3 A (where discharging is positive and charging is negative). The external charging power source is an ideal voltage source in series with a resistor. The output currents of the batteries in the nine BUCs were set to be shared in two ratios, called mode 1 and mode 2. Data for both modes are given in Table III.

Fig. 13 shows the charging simulation waveforms for mode 2, which is similar to mode 1. From top to bottom, the five

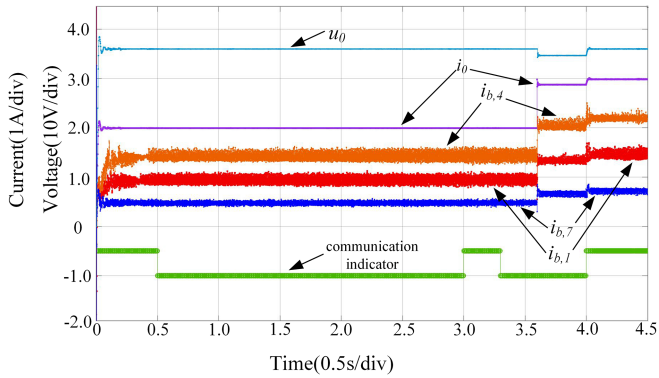


Fig. 14. Simulation experiment of communication failure.

waveforms in Fig. 13 are the battery output current $i_{b,7}$ of the seventh BUC, the battery output current $i_{b,1}$ of the first BUC, the battery output current $i_{b,4}$ of the fourth BUC, the total output current $i_0$, and the total output voltage $u_o$. For better display, $u_o$ is multiplied by −0.1. The total output current $i_0$ and total output voltage $u_o$ reach steady state at approximately 0.1 s, while the output currents of the batteries reach steady state at around 0.15 s. After reaching steady state, the average total output current $i_0$ is −3.000 A with zero error, and the current ripple amplitude percentage is 0.95%. The total output voltage $u_o$ is 35.83 V with a voltage ripple amplitude percentage of 0.14%.The current sharing errors of the battery output currents are no more than 0.30%, with the average percentage of battery output current ripple amplitude being 8.4%, the minimum value 5.7%, and the maximum value 14.0%.

### C. Simulation Experiment of Communication Failure

To verify the system's stability, a simulation experiment of communication failure was conducted under constant voltage discharging condition. The total output voltage is set to 36 V. Fig. 14 shows the waveforms of the communication failure experiment. From top to bottom, the six waveforms are the total output voltage $u_o$, the total output current $i_0$, the battery output current $i_{b,4}$ of the fourth BUC, the battery output current $i_{b,1}$ of the first BUC, the battery output current $i_{b,7}$ of the seventh BUC, and the communication indicator signal, where a high level indicates normal communication, and a low level indicates communication failure. As seen in Fig. 14, the system reaches a steady state at 0.15 s. At 0.5 s, a communication failure occurs. At this point, the total output voltage, the total output current, and the output currents of each battery remain stable without significant changes. At 3.0 s, communication resumes, and the 2.5 s communication failure has no significant impact on the voltage and current variables in the system. At 3.3 s, the second communication failure occurs. At 3.6 s, the load resistance suddenly changes, causing the total output current to increase from 1.994 to 2.875 A. During this time, without the upper control strategy, the system is governed by the lower droop control, resulting in the total output voltage decreasing from 36.00 to 34.67 V, and the output currents of each battery

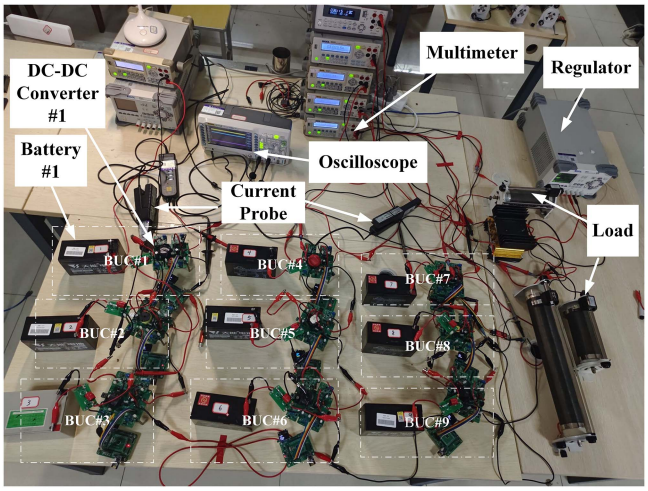


Fig. 15. Experimental platform of nine BUCs.

TABLE IV
COMPONENT PARAMETERS OF THE EXPERIMENT

| Device | Parameter |
|---|---|
| No. 3 lead-acid battery | 12V，12Ah |
| No. 6 lead-acid battery | 12V，9Ah |
| No. 1, 2, 4, 5, 7, 8, 9 lead-acid Batteries | 12V，7Ah |
| Switching frequency | 20kHz |
| MCU chip | STM32G030C8 |
| MOSFET | IRF2807 |
| Half-bridge driver ICs | IR2104 |
| Current measurement chips | INA240 |
| Wireless communication chips | NRF24L01 |

increasing proportionally. At 4.0 s, communication resumes again, and the total output voltage returns to the set value of 36.00 V. As the total output voltage slightly increases, the total output current also rises to 2.986 A, and the output currents of each battery increase slightly in proportion.

## VIII. EXPERIMENTAL VERIFICATION

To construct an experimental platform, nine BUCs were first connected in three series groups with three batteries included in every series group, and then these series groups were connected in parallel, as shown in Fig. 15. Each BUC in the experiment includes a lead-acid battery with a rated voltage of 12 V and an electrical part. The electrical part of each BUC includes the following modules: dc–dc circuit, microcontroller control circuit, communication circuit, current measurement circuit, voltage measurement circuit, and drive circuit. The capacities, brands, and aging conditions of the batteries in the nine BUCs are not completely identical. This system demonstrates good adaptability to different battery types, which is one of the common advantages of balancing technology based on modular converters. The component parameters of the experiments are shown in Table I and Table IV. The initial droop function for each BUC is: $u = 13.5 - 1.5i$.

TABLE V
DISCHARGING EXPERIMENT

| | $i_{b\_rati\text{-}o\_ref}$ | $i_b$/A | Current sharing error | Total Output Voltage (V) | Total Output Voltage Error |
|---|---|---|---|---|---|
| Mode 1 | 1 1 1 | 1.064 1.108 1.065 | | | |
| | 1 1 1 | 1.061 1.071 1.070 | 0.91% | 35.90 | 0.28% |
| | 1 1 1 | 1.067 1.047 1.062 | | | |
| Mode 2 | 2 3 1 | 1.626 2.422 0.809 | | | |
| | 1 1 1 | 0.807 0.794 0.811 | 0.94% | 35.92 | 0.22% |
| | 1 1 1 | 0.791 0.792 0.798 | | | |

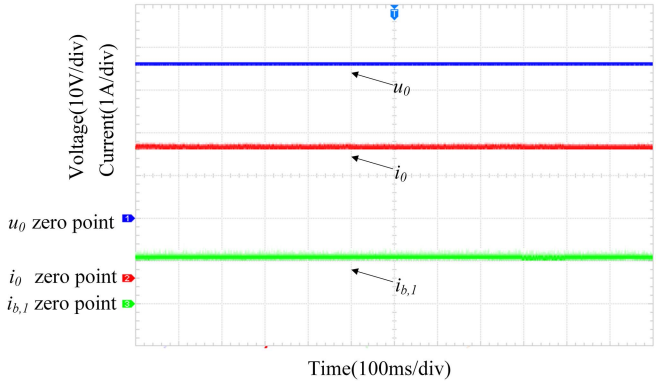


Fig. 16. Waveforms of discharging experiment.

### A. Discharging Experiment

The energy storage system was discharged at a constant voltage, with the total output voltage set to 36 V and the load resistance at 12 Ω. The output currents of the batteries in the nine BUCs were set to be shared in two ratios, called mode 1 and mode 2. Data for both modes are given in Table V, where voltage and current data was measured using a multimeter. Fig. 16 shows the discharging experiment waveforms for mode 1, which is similar to mode 2. The current waveforms were measured using two Tektronix A622 current probes. From top to bottom, the three waveforms in Fig. 16 are the total output voltage $u_{o,}$ the total output current $i_0$, and the battery output current $i_{b,1}$ of the first BUC. After reaching steady state, the average value and error of the total output voltage $u_o$ for mode 1 and mode 2 are given in Table V. The average total output currents $i_0$ for the two modes are 2.994 A and 3.004 A, respectively. The current sharing errors of the battery output currents are no more than 0.94%, with the average percentage of ripple amplitudes of battery output currents being about 11.3%, the minimum value about 7.3%, and the maximum value about 15.1%. Under the effect of the input filter, the ripple at the PWM switching frequency is reduced to about 0.034 A, which is negligible. The main component of the battery output current ripple, with a period of milliseconds, cannot be completely eliminated.

### B. Charging Experiment

The energy storage system was charged at a constant current, with the total output current set to −3 A (where discharging is positive and charging is negative). The output currents of the

TABLE VI
CHARGING EXPERIMENT

| | $i_{b}$_rati-o_ref | $i_b$/A | Current sharing error | Total output current (A) | Total output current error |
|---|---|---|---|---|---|
| Mode 1 | 1 1 1 | -0.790 -0.798 -0.814 | | | |
| | 1 1 1 | -0.775 -0.783 -0.785 | 1.17% | -3.015 | 0.50% |
| | 1 1 1 | -0.780 -0.778 -0.779 | | | |
| Mode 2 | 2 3 1 | -1.265 -1.827 -0.606 | | | |
| | 1 1 1 | -0.528 -0.589 -0.580 | 2.48% | -2.987 | 0.43% |
| | 1 1 1 | -0.601 -0.579 -0.586 | | | |

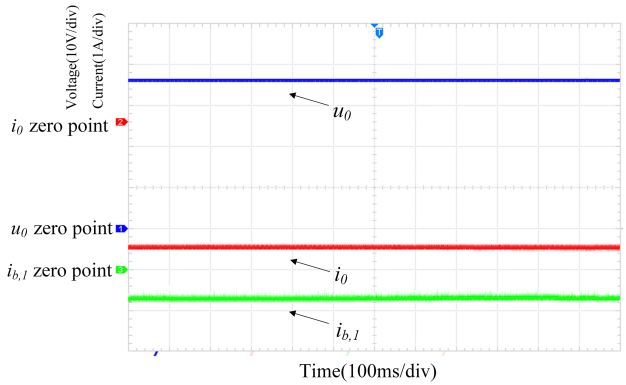


Fig. 17. Waveforms of charging experiment.

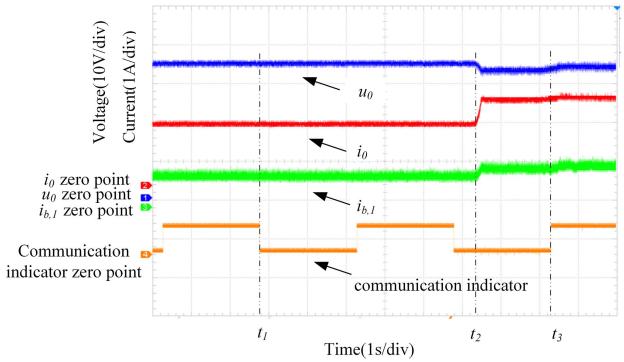


Fig. 18. Communication failure experiment.

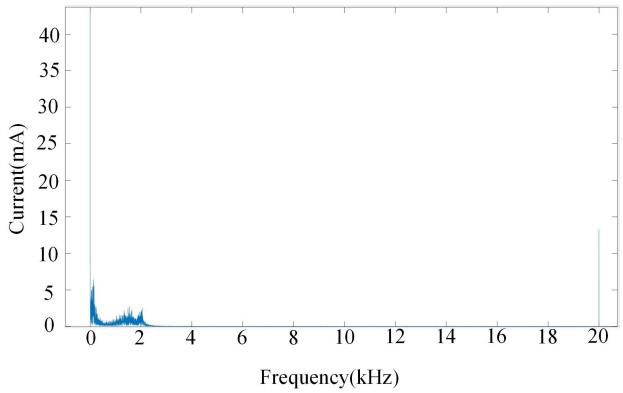


Fig. 19. Spectrum of battery output current.

batteries in the nine BUCs were set to be shared in two ratios, called mode 1 and mode 2. Data for both modes are given in Table VI. Fig. 17 shows the charging experiment waveforms for mode 1, which is similar to mode 2. From top to bottom, the three waveforms in Fig. 17 are the total output voltage $u_o$, the total output current $i_0$, and the battery output current $i_{b,1}$ of the first BUC. After reaching steady state, the errors of the total output current $i_0$ are no more than 0.50%. The current sharing errors of the battery output currents are no more than 2.48%, with the average percentage of ripple amplitudes of battery output currents being about 10.7%.

### C. Communication Failure Experiment

To verify the system's stability, a communication failure experiment was conducted under constant voltage discharging condition mode 2. The total output voltage was set to 36 V. Fig. 18 shows the waveforms of the communication failure experiment. From top to bottom, the four waveforms are the total output voltage $u_{o,}$ the total output current $i_0$, the battery output current $i_{b,1}$ of the first BUC, and the communication indicator signal, where a high level indicates normal communication, and a low level indicates communication failure. As seen in Fig. 18, at time $t_1$, a communication failure occurs. At this point, the total output voltage, the total output current, and the output currents of each battery remain stable without significant changes. The 2.5 s communication failure has no significant impact on the voltage and current variables in the system. During the second communication failure, at time $t_2$, the load resistance suddenly changes, causing the total output current to increase from 1.591 to 2.124 A. During this time, without the upper control strategy, the system is governed by the lower droop control, resulting in the total output voltage decreasing from 35.86 to 33.78 V, and the output currents of each battery increasing proportionally. At time $t_3$, communication resumes again, and the total output voltage returns to the set value, and the measured value of $u_o$ is 35.85 V. As the total output voltage slightly increases, the total output current also rises to 2.254 A, and the output currents of each battery increase slightly in proportion.

## IX. DISCUSSIONS

### A. Discussions on Voltage and Current Ripples

The scheme proposed in this article involves a battery output current $i_{b,k}$, which is the input current to the dc–dc converter and has ripples. These ripples consist of two main components: high-frequency ripples at the switching frequency and millisecond-scale stray ripples. By adding a small-capacity inductor to the dc–dc input, forming an input *LC* filter, the high-frequency ripple at the switching frequency has been controlled within an acceptable and reasonable range. By optimizing the control loop parameters, such as appropriately reducing the sampling adjustment interval time $\tau$ of the current loop, the millisecond-scale stray ripples are also reduced to some extent. As shown in Fig. 19, the amplitude–frequency plot of the battery current $i_{b,1}$ in BUC1 has a 20 kHz switching frequency component of approximately 14 mA, and there are also some millisecond-scale stray ripples with the maximum amplitude of about 6.5 mA. The

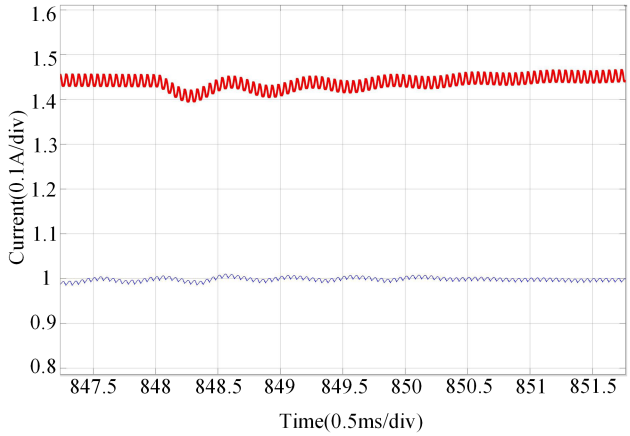


Fig. 20. Current ripples of simulation.

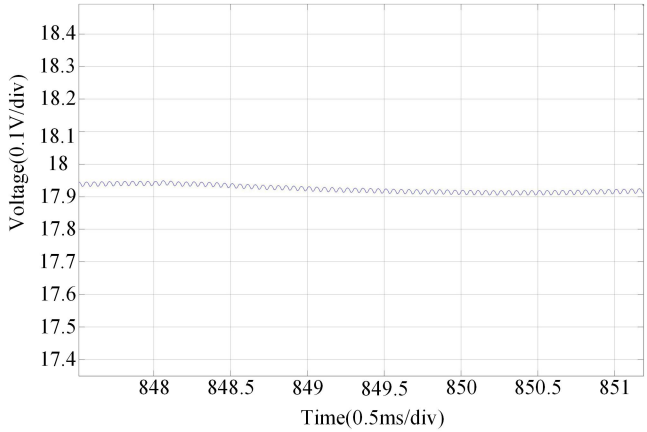


Fig. 21. Output voltage ripples of simulation.

dc amplitude is 1.435 A, which exceeds the display range of the graph.

Figs. 20 and 21 show the waveforms of constant voltage discharge simulation experiments.

In Fig. 20, the top waveform represents $i_{b,1}$, whose ripple peak-to-peak value is about 80 mA, accounting for about 5.6% of the fundamental wave. The lower waveform represents the dc–dc output current $i_1$ in BUC1, with a ripple peak-to-peak value of about 20 mA, accounting for about 2.0% of the fundamental wave. Fig. 21 shows the waveform of the dc–dc output voltage $u_1$ in BUC1, with a ripple peak-to-peak value of about 45 mV, accounting for about 0.3% of the fundamental wave.

Fig. 22 shows the waveform of a constant voltage discharge experiment. The top waveform represents $i_{b,1}$, with a ripple peak-to-peak value of about 110 mA, accounting for about 6.8% of the fundamental wave. The middle waveform represents the dc–dc output current $i_1$ in BUC1, with a ripple peak-to-peak value of about 60 mA, accounting for about 5.9% of the fundamental wave. The lower waveform represents the dc–dc output voltage $u_1$ in BUC1, with a ripple peak-to-peak value of about 250 mV, accounting for about 1.4% of the fundamental wave.

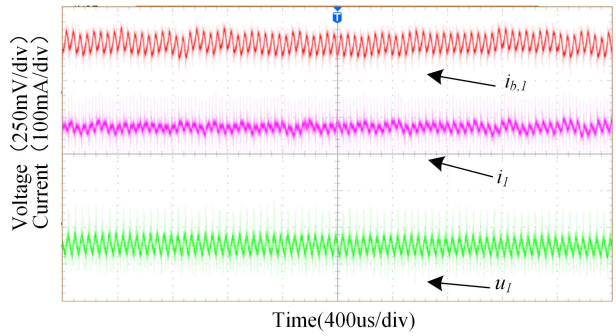


Fig. 22. Voltage and current ripples of physical experiment.

Although the ripple of the battery output current $i_{b,k}$ has been reduced to some extent, it cannot be completely eliminated, nor is it necessary to eliminate it entirely. This is because, in the scheme proposed in this article, the output of the dc–dc converter is more important than the input. The stability and control accuracy of the output determine the overall output control accuracy of the energy storage system and the power distribution control accuracy between modules. Therefore, the controlled variables in the lower control strategy proposed in this article are the voltage $u_k$ and current $i_k$ at the output terminal of the dc–dc converter rather than the battery current $i_{b,k}$ at the input terminal. The instantaneous values of $u_k$ and $i_k$ are controlled and stable, while the instantaneous values of $i_{b,k}$ are only passively stable, not actively controlled. As a result, the stability of the instantaneous value of $i_{b,k}$ is lower than that of the voltage $u_k$ and current $i_k$ at the output terminal of the dc–dc converter. However, the stability of the effective value and integral value of $i_{b,k}$ is the same as that of the voltage $u_k$ and current $i_k$ at the output terminal of the dc–dc converter, which can be explained by the following principles.

Ignoring the losses in the dc–dc converter, the conservation of instantaneous power and active power can be expressed by the following two equations:

$$u_{b,k} i_{b,k} = u_k i_k + p \tag{66}$$

$$U_{b,k} I_{b,k} = U_k I_k. \tag{67}$$

Integrating both sides of (66) yields

$$u_{b,k} \int_0^t i_{b,k} dt = \int_0^t u_k i_k dt. \tag{68}$$

In (66), $p$ represents the sum of the reactive power instantaneous values of the inductors and capacitors in the dc–dc converter; in (67), $U_{b,k}$ and $I_{b,k}$ are the RMS values of the battery output voltage and current, respectively, while $U_k$ and $I_k$ are the RMS values of the dc–dc output voltage and current, respectively. Equation (66) shows that due to the influence of the reactive power $p$, the stability and control accuracy of the instantaneous value of $i_{b,k}$ are lower than those of the dc–dc output voltage $u_k$ and current $i_k$. Equation (67) shows that the stability and control accuracy of the RMS value of $i_{b,k}$ are the same as those of $u_k$ and $i_k$ .Since $u_k$ and $i_k$ in the proposed scheme have high stability and control accuracy, the stability

and control accuracy of the RMS value of $i_{b,k}$ are also high, which had been verified in the experiments. Over a short period, it is assumed that the battery voltage is constant. According to (68), the stability and control accuracy of the integral value of $i_{b,k}$ are the same as those of $u_k$ and $i_k$, and therefore, the stability and control accuracy of the integral value of $i_{b,k}$ are also high. Since the change in the SOC of the battery is the integral value of $i_{b,k}$, the control of SOC also has high accuracy. In summary, the proposed scheme in this article achieves high control accuracy for the RMS and integral values of the battery current $i_{b,k}$. As a result, the control of the battery's output active power and SOC is also highly accurate. Although the stability of the instantaneous value of $i_{b,k}$ is slightly lower, it is still within a reasonable range and does not affect the normal operation of the battery. In addition, since it is an internal variable, it has no adverse impact on the system's output.

Furthermore, through further analysis of the system's control stability, a deeper understanding of the working mechanism of the parallel BUCs has been obtained. An empirical formula for the dc–dc output voltage ripple amplitude caused by the current loop control strategy in the parallel BUCs has been derived

$$2\mathrm{U}_m = \tau \frac{du_k}{dt}. \tag{69}$$

In (69), $\tau$ *i*s the sampling adjustment interval time of the current loop, $U_m$ is the amplitude of the dc–dc output voltage ripple caused by the current loop control strategy, and d$u_k$/d$t$ is the derivative of the dc–dc output voltage, the rate of change of the voltage.

### *B. Comparison Between the Proposed Solution and Existing Technologies*

*1) Classification and Comparison of Existing Technologies:* The field studied in this article pertains to modular battery energy storage systems. The main problem to be solved is the control of series and parallel modular converters, with the control objective being: to maintain a constant output voltage or a constant output current for the entire energy storage system; and to distribute the output current of each battery according to a given ratio. Existing literature on this issue includes the works presented in [13], [14], [15], [16], [17], [18], [19], [20], [21], [22], [23], [24], and [25], which come from high-quality academic journals, including both recent publications and historically influential ones. These references cover various technical approaches aimed at solving the problem and represent the most advanced existing technologies in this field. In Table VII, the existing state-of-the-art technologies are classified and compared from the perspective of overall control methods. The evaluation levels are divided into five grades, from high to low as follows: very high (VH), high (H), medium (M), low (L), very low (VL).

*Class 1: Centralized Control* [13], [16]

This method provides very high control accuracy because it does not require communication, thus offering good adaptability to communication failures. However, the drawback of centralized control schemes is their poor scalability and lack of fault tolerance. If the central controller fails, the entire system will stop operating.

TABLE VII
CLASSIFICATION AND COMPARISON OF THE STATE-OF-THE-ART TECHNOLOGY

| Class | Classification | | Representative literature | Control accuracy | Adaptability to communication failures | Scalability | Fault-tolerant operation capability |
|---|---|---|---|---|---|---|---|
| 1 | Centralized control | | [13] [16] | VH | VH | L | L |
| 2 | Distributed control without communication | | [17] [18] [19] | M | VH | H | H |
| 3 | Distributed control with communication | 3.1 Without droop control | [15] [20] | VH | M | H | VH |
| | | 3.2 With droop control | [21] [22] [23] | VH | M | H | VH |
| | | | This article | VH | VH | VH | VH |
| 4 | Hybrid control | | [24] [25] | VH | M | H | H |

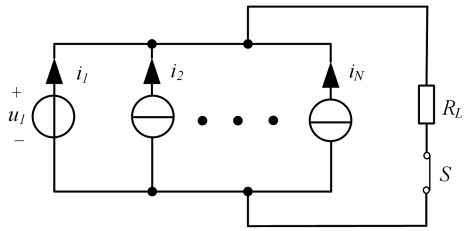


Fig. 23. Overcurrent impact principle of Class 3.1 Schemes.

*Class 2: Distributed Control without Communication* [17], [18], [19]

This method employs droop control and has excellent adaptability to communication failures. However, its control accuracy is lower. The current technology has primarily focused on series or parallel configurations but has not yet proposed solutions that can simultaneously extend both series and parallel connections. In addition, this type of system does not meet the need for communication in battery energy storage systems for state monitoring.

*Class 3: Distributed Control With Communication*

This class is divided into two subcategories.

*Class 3.1:* In these solutions, each modular converter is set to operate in either voltage source or current source mode. The system functions by controlling the set values of the voltage and current sources. While these solutions have high accuracy, their major drawback is that, in the event of a communication failure, if the load current fluctuates, overcurrent or overvoltage surges may occur. This can be illustrated using an equivalent circuit as shown in Fig. 23, where during normal operation, branch currents are equal, and when the load switch is turned OFF, the voltage source branch experiences a current surge of ($n$-1) times.

This article also falls into Class 3.2. While solutions in this class have high control accuracy, there are no existing

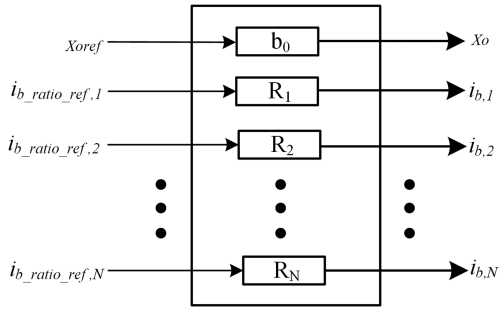


Fig. 24. MIMO system model.

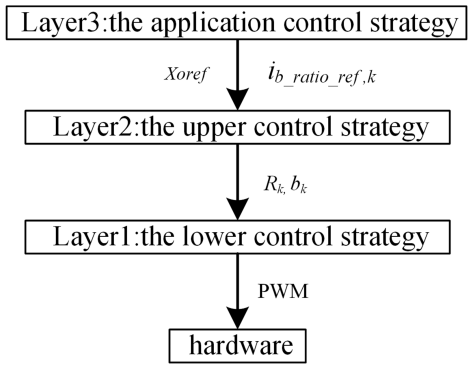


Fig. 25. Layers of the control strategies.

schemes that simultaneously extend both series and parallel configurations using the same control strategy. In addition, these schemes do not adapt well to communication failures. In [22], the experiments have been conducted on the impact of communication failures on system stability, indicating that the system can operate normally when communication failures are less than 20 ms but fails to operate when communication failures exceed 1 s. The experiments are well considered and persuasive. The main advantage of the improved scheme proposed in this article is its excellent adaptability to communication failures and its flexibility in extending both series and parallel configurations.

*Class 4: Hybrid Control Refers to the Use of Two Different Control Methods*

The innovation in [24] lies in the proposal of a modular battery energy storage system scheme that can be extended both in series and parallel. It uses centralized control in the parallel group and leader/follower control with communication in the series group. The innovation in [25] is mainly that the output operates in current source mode, making parallel connections easier while eliminating the need for output current detection circuits. It uses centralized control in the parallel group and droop control with communication in the series group. Although innovations lie in [24] and [25], their control methods still fall under the centralized control and communication-based distributed control categories. Therefore, their adaptability to communication failures and scalability are somewhat lower.

*2) Main Reasons Why the Proposed Scheme Improves on Existing Technologies:* In addressing the control issues of series and parallel modular converters in modular battery energy storage systems, this article improves the adaptive droop control approach and proposes a variant of droop control suitable for series and parallel expansion. In addition, a two-layer composite control strategy is introduced, which maintains high control precision while enhancing adaptability to communication failures. Due to this enhanced adaptability, wireless communication can be employed, further improving scalability. The main reason the proposed scheme can achieve these improvements lies in decoupling, which occurs in two aspects.

*First Aspect of Decoupling: Decoupling of Input and Output Variables*

As shown in Fig. 24, the control object in this article can be regarded as a multi-input, multioutput system. Suppose the system consists of $N$ battery power modules. The input variables include the reference values of the total output voltage or current of the energy storage system $X_{\mathrm{oref}}$ and the reference values of the output current ratios of all batteries $i_{b\_\mathrm{ratio\_ref},k}$. The output variables include the total output voltage or current of the energy storage system $X_o$ and the output current of each battery $i_{b,k}$. The intermediate control variables are the equivalent droop open-circuit voltage $b_0$ of the energy storage system and the droop resistance $R_k$ of each BUC. The input, output, and intermediate variables in the proposed scheme are decoupled. The total output $X_o$ is only related to $X_{\mathrm{oref}}$ and $b_0$, and the output current of each battery $i_{b,k}$ is only related to $i_{b\_\mathrm{ratio\_ref},k}$ and $R_k$ within the same group. Therefore, the proposed scheme is a weakly coupled system, whereas similar existing schemes are strongly coupled systems, which are more susceptible to communication failure interference. For instance, in [22], both the output voltage and current control rely on regulating the droop open-circuit voltage, making it a typical strongly coupled system. As such, its adaptability to communication failures is lower: when communication failure is less than 20 ms, the system can operate normally, but when communication failure exceeds 1 s, the system cannot function correctly.

*Second Aspect of Decoupling: Decoupling of Control Strategy*

The proposed scheme also adopts a hierarchical control strategy, decoupling the control strategies at each layer. As shown in Fig. 25, when applied to the BMS, the control strategy is divided into three layers: the application control strategy, the upper control strategy, and the lower control strategy. The application control strategy runs algorithms for SOC balancing, battery thermal management, or active safety management of the battery. Its outputs include the reference values for the total output of the energy storage system $X_{\mathrm{oref}}$ and the reference values of the output current ratios of all batteries $i_{b\_\mathrm{ratio\_ref},k}$. The upper control strategy receives the output from the application control strategy as input, and based on the reference value $X_{\mathrm{oref}}$, the measured value $X_o$, the reference values of the output current ratios of each battery $i_{b\_\mathrm{ratio\_ref},k}$, and the measured values of the output current of each battery $i_{b,k}$, it calculates the droop open-circuit voltages $b_k$ and droop resistances $R_k$ of each BUC. These values are then output to the lower control strategy. The lower control strategy, based on $b_k$, $R_k$, and the output voltage and current of each BUC, calculates the PWM signals and sends them to the hardware.

The layers of the proposed control strategy are linked through simple instruction data, and their control loops are independent, making it a weakly coupled system. This structure provides better adaptability to communication failures. In addition, because the algorithms at each layer are independent, the system's flexibility is enhanced, making it easier to develop a variety of powerful battery management algorithms. In contrast, existing compared technologies often couple the algorithms of all three layers together, which lead to a strongly coupled system, reducing both adaptability to communication failures and the flexibility of the algorithms.

### C. Discussion on Target Application Scenarios

Before discussing the target application scenarios of this article, let us first introduce the ultimate research goal. The BUC proposed in this article is just the first step. The ultimate research goal of this article is to transform the BUC into the battery robot (BR). The construction method and control strategy of the BUC-based energy storage system are foundational to the BR system. However, there are still many interesting topics that need further research as we transition from BUC to BR.

The BR integrates batteries, measurement circuits, communication circuits, embedded AI, and modular converters. The measurement and communication circuits act as the "nervous system" of the BR, enabling it to be perceptive and communicative. Embedded AI serves as the "brain," giving the BR the ability to think. The modular converter functions as the "muscle," providing the BR with the ability to act. However, the actions of the BR are not mechanical motions but rather electrical motions, specifically reflected in its ability to control output voltage and current.

In the concept of the BR, the battery is no longer an uncontrollable electrochemical device but becomes an "intelligent beings" capable of perception, communication, thought, and action. The energy storage system based on BRs is made up of many small BRs working together in coordination, which has the potential to change the construction model of current battery energy storage systems. BRs have broad application prospects in battery and supercapacitor energy storage systems and can be used in scenarios such as 5G base station energy storage, home energy storage, commercial and industrial energy storage, electric vehicles, and more.

## X. Conclusion

Currently, the balancing technology based on modular converters faces challenges such as poor adaptability to communication failures, stability issues, and scalability limitations. The BUC-based energy storage system proposed in this article is expected to address these issues; furthermore, it maybe evolves into a new architecture for energy storage systems. This architecture opens avenues for further research, including topics such as SOC balancing strategies specific to BUC-based energy storage systems, intelligent batteries, fault-tolerant operation of energy storage systems, and wireless communication self-organizing network technologies for BUC-based energy storage systems. From the following perspective, the next research of this article maybe will get more inspiration: When humans manufacture a product, they first manufacture the various macroparts of the product and then assemble them, which is a kind of manufacturing at the macrolevel. However, the construction of organisms by nature is a kind of microlevel manufacturing, which first constructs cells with certain functions, and then constructs organisms by these cells working together. The BUC proposed in this article can be regarded as an energy storage "cell," and a new architecture of energy storage systems can be developed by the cooperation of these energy storage "cells."

## References


[1] M. Rouholamini et al., "A review of modeling, management, and applications of grid-connected Li-ion battery storage systems," *IEEE Trans. Smart Grid*, vol. 13, no. 6, pp. 4505–4524, Nov. 2022, doi: 10.1109/TSG.2022.3188598.

[2] D. Shen et al., "Detection and quantitative diagnosis of micro-short-circuit faults in lithium-ion battery packs considering cell inconsistency," *Green Energy Intell. Transp.*, vol. 2, no. 5, Jul. 2023, Art. no. 100109, doi: 10.1016/j.geits.2023.100109.

[3] F. A. R. Vija, S. Cregut, G. Z. Papadopoulos, N. Montavont, and R. Group, "From wired to wireless BMS in electric vehicles," in *Proc. 17th Int. Conf. Mobility, Sens. Netw.*, Exeter, U.K., 2021, pp. 255–262, doi: 10.1109/MSN53354.2021.00049.

[4] H. Li, M. Bin Kaleem, Z. Liu, Y. Wu, W. Liu, and Z. Huang, "IoB: Internet-of-batteries for electric vehicles – Architectures, opportunities, and challenges," *Green Energy Intell. Transp.*, vol. 2, no. 6, Dec. 2023, Art. no. 100128, doi: 10.1016/j.geits.2023.100128.

[5] Z. Zhao, H. Hu, Z. He, H. H.-C. Iu, P. Davari, and F. Blaabjerg, "Power electronics-based safety enhancement technologies for lithium-ion batteries: An overview from battery management perspective," *IEEE Trans. Power Electron.*, vol. 38, no. 7, pp. 8922–8955, Jul. 2023, doi: 10.1109/TPEL.2023.3265278.

[6] Y. Izadi and R. Beiranvand, "A comprehensive review of battery and supercapacitor cells voltage-equalizer circuits," *IEEE Trans. Power Electron.*, vol. 38, no. 12, pp. 15671–15692, Dec. 2023, doi: 10.1109/TPEL.2023.3310574.

[7] U. Abronzini, M. Di Monaco, F. Porpora, G. Tomasso, M. D'Arpino, and C. Attaianese, "Thermal management optimization of a passive BMS for automotive applications," in *Proc. AEIT Int. Conf. Elect. Electron. Technol. Automot.*, Turin, Italy, Jul. 2019, pp. 1–6, doi: 10.23919/EETA.2019.8804559.

[8] Y. Shang, C. Zhang, N. Cui, and C. Mi, "A delta-structured switched-capacitor equalizer for series-connected battery strings," *IEEE Trans. Power Electron.*, vol. 34, no. 1, pp. 452–461, Jan. 2018, doi: 10.1109/TPEL.2018.2826010.

[9] X. Zheng, X. Liu, Y. He, and G. Zeng, "Active vehicle battery balancing scheme in the condition of constant-voltage/current charging and discharging," *IEEE Trans. Veh. Technol.*, vol. 66, no. 5, pp. 3714–3723, May 2017, doi: 10.1109/TVT.2016.2609920.

[10] S. Li, C. C. Mi, and M. Zhang, "A high-efficiency active battery-balancing circuit using multiwinding transformer," *IEEE Trans. Ind. Appl.*, vol. 49, no. 1, pp. 198–207, Jan. 2013, doi: 10.1109/TIA.2012.2229455.

[11] S. Jinlei, L. Wei, T. Chuanyu, W. Tianru, J. Tao, and T. Yong, "A novel active equalization method for series-connected battery packs based on clustering analysis with genetic algorithm," *IEEE Trans. Power Electron.*, vol. 36, no. 7, pp. 7853–7865, Jul. 2021, doi: 10.1109/TPEL.2021.3049166.

[12] H.-D. Gui, Z. Zhang, D.-J. Gu, Y. Yang, Z. Lu, and Y.-F. Liu, "A hierarchical active balancing architecture for Li-ion batteries," in *Proc. IEEE Appl. Power Electron. Conf. Expo.*, Long Beach, CA, USA, Mar. 2016, pp. 1243–1248, doi: 10.1109/APEC.2016.7468027.

[13] W. Huang and J. A. Abu Qahouq, "Energy sharing control scheme for State-of-charge balancing of distributed battery energy storage system," *IEEE Trans. Ind. Electron.*, vol. 62, no. 5, pp. 2764–2776, May 2015, doi: 10.1109/TIE.2014.2363817.

[14] Z. Zhang, Y.-Y. Cai, Y. Zhang, D.-J. Gu, and Y.-F. Liu, "A distributed architecture based on microbank modules with self-reconfiguration control to improve the energy efficiency in the battery energy storage system," *IEEE Trans. Power Electron.*, vol. 31, no. 1, pp. 304–317, Jan. 2016, doi: 10.1109/TPEL.2015.2406773.

[15] Y. Li and Y. Han, "A module-integrated distributed battery energy Storage and Management system," *IEEE Trans. Power Electron.*, vol. 31, no. 12,pp. 8260–8270, Dec. 2016, doi: 10.1109/TPEL.2016.2517150.
[16] M. Uno, D. Cheng, S. Onodera, and Y. Sasama, "Bidirectional buck-boost converter using cascaded energy storage modules based on cell voltage equalizers," *IEEE Trans. Power Electron.*, vol. 38, no. 1, pp. 1249–1261, Jan. 2023, doi: 10.1109/TPEL.2022.3203900.
[17] X. Lu, K. Sun, J. M. Guerrero, J. C. Vasquez, and L. Huang, "Double-quadrant State-of-charge-based droop control method for distributed energy storage systems in autonomous DC microgrids," *IEEE Trans. Smart Grid*, vol. 6, no. 1, pp. 147–157, Jan. 2015, doi: 10.1109/TSG.2014.2352342.
[18] S. M. Chowdhury, M. O. Badawy, Y. Sozer, and J. A. D. A. Garcia, "A novel battery management system using the duality of the adaptive droop control theory," *IEEE Trans. Ind. Appl.*, vol. 55, no. 5, pp. 5078–5088, Sep. 2019, doi: 10.1109/TIA.2019.2919497.
[19] S. Chowdhury, M. N. B. Shaheed, and Y. Sozer, "State-of-charge balancing control for modular battery system with output DC bus regulation," *IEEE Trans. Transport. Electrific.*, vol. 7, no. 4, pp. 2181–2193, Dec. 2021, doi: 10.1109/TTE.2021.3090735.
[20] R. Bhosale, R. Gupta, and V. Agarwal, "A novel control strategy to achieve SOC balancing for batteries in a DC microgrid without droop control," *IEEE Trans. Ind. Appl.*, vol. 57, no. 4, pp. 4196–4206, Jul. 2021, doi: 10.1109/TIA.2021.3073376.
[21] K. Bi, S. Zhang, Y. Zhu, W. Huang, W. Lu, and Q. Fan, "An improved SOC balancing strategy for HVDC modular energy storage system based on low bandwidth communication with enhanced current regulation accuracy," *IEEE Trans. Energy Convers.*, vol. 36, no. 4, pp. 3355–3364, Dec. 2021, doi: 10.1109/TEC.2021.3082300.
[22] X. Lu, J. M. Guerrero, K. Sun, and J. C. Vasquez, "An improved droop control method for DC microgrids based on low bandwidth communication with DC bus voltage restoration and enhanced current sharing accuracy," *IEEE Trans. Power Electron.*, vol. 29, no. 4, pp. 1800–1812, Apr. 2014, doi: 10.1109/TPEL.2013.2266419.
[23] M. Mokhtar, M. I. Marei, and A. A. El-Sattar, "An adaptive droop control scheme for DC microgrids integrating sliding mode voltage and current controlled boost converters," *IEEE Trans. Smart Grid*, vol. 10, no. 2, pp. 1685–1693, Mar. 2019, doi: 10.1109/TSG.2017.2776281.
[24] Y. Cao and J. A. Abu Qahouq, "Hierarchical SOC balancing controller for battery energy storage system," *IEEE Trans. Ind. Electron.*, vol. 68, no. 10, pp. 9386–9397, Oct. 2021, doi: 10.1109/TIE.2020.3021608.
[25] M. Kamel, V. Sankaranarayanan, R. Zane, and D. Maksimovic, "State-of-charge balancing with parallel and series output connected battery power modules," *IEEE Trans. Power Electron.*, vol. 37, no. 6, pp. 6669–6677, Jun. 2022, doi: 10.1109/TPEL.2022.3143835.

**Chao Wang** (Member, IEEE) received the B.Sc. degree in thermal power engineering from Wuhan University, Wuhan, China, in 2001, and the M.Sc. degree in electrical engineering from Zhejiang University, Hangzhou, China, in 2004.

He was a Research Engineer with Haixin Research and Design Center in 2004, and an Embedded Software Engineer with Huawei 3G Wireless Communication Product Line in 2005. Since 2006, he has been with the School of Electrical and Electronic Engineering, Hubei University of Technology, Wuhan, China, where he is currently an Associate Professor. From 2008 to 2017, he was a Chief Engineer with Masterlyelec, Co., Ltd. His research interests include power electronics for energy storage systems and renewable energy, IOT, and embedded AI systems.

**Qiangxiang Zhang** received the B.Sc. degree in electrical engineering and automation from the Wuchang University of Technology, Wuhan, China, in 2018. He is currently working toward the master's degree in electrical engineering with the Hubei University of Technology, Wuhan, China.

His main research interest focuses on energy storage technology.

**Li Han** received the B.Sc. degree in electrical engineering and automation from Hefei Normal University, Hefei, China, in 2021. He is currently working toward the master's degree in electrical engineering with the Hubei University of Technology, Wuhan, China.

His main research interests include energy storage technology.

**Yiping Xiao** (Member, IEEE) was born in Hubei, China, in 1973. She received the M.Sc. degree in power electronics and power transmission and the Ph.D. degree in transportation information engineering and control from the Wuhan University of Technology, Wuhan, China, in 2008 and 2011, respectively.

Since 2011, she has been working as a Lecturer with the Hubei University of Technology, Wuhan, China. Her current research interests include renewable energy generation, grid connection, and power electronics.

**Kang Xie** is currently working toward the B.Sc. degree in electrical engineering with the Hubei University of Technology, Wuhan, China.

Mr. Xie was a recipient of the First Prize in 2023 National Undergraduate Electronic Design Contest of China.

**Tiezhou Wu** received the B.Sc. degree in electronics and information engineering from Wuhan University, Wuhan, China, in 1988, the M.Sc. degree in electrical engineering from the Naval University of Engineering, Wuhan, China, in 2003, and the Ph.D. degree in systems analysis and integration from the Huazhong University of Science and Technology, Wuhan, China, in 2010.

From 1989 to 1999, he was an Engineer with Wuhan Science and Technology Bureau. Since 2003, he has been with the School of Electrical and Electronic Engineering, Hubei University of Technology, Wuhan, China, where he is currently a Professor. He is the Director of the Hubei Key Laboratory for High-Efficiency Utilization of Solar Energy and Operation Control of Energy Storage System. His research interests include battery energy storage systems and solar photovoltaic systems.

**Mengjun Liang** (Member, IEEE) received the B.Sc. and M.Sc. degrees in chemical engineering from Hubei Normal University, Huangshi, China, in 2012 and 2016, respectively, and the Ph.D. degree in electronic science and technology from South China Normal University, Guangzhou, China, in 2019.

She is currently working with the School of Electrical and Electronic Engineering, Hubei University of Technology, Wuhan, China. Her research interests include semiconductor devices, electrochemical and photoelectrochemical energy storage systems, and seawater desalination.